Spatial patterns of neuroimaging biomarker change in individuals from families with autosomal dominant Alzheimer disease: a longitudinal study

Brian A. Gordon*[+][a,b], PhD, Tyler M. Blazey[+][c], BS, Yi Su[a], PhD, Amrita Hari-Raj[a], BA, Aylin Dincer[a], BA, Shaney Flores[a], BS, Jon Christensen[a], BS, Eric McDade[c,d], DO, Guoqiao Wang[d], PhD, Prof. Chengjie Xiong[b,e], PhD, Prof. Nigel J. Cairns[b,d], PhD, Jason Hassenstab[b,d,f], PhD, Daniel S. Marcus[a], PhD, Prof. Anne M. Fagan[b,d,g], PhD[d], Prof. Clifford R. Jack Jr.[h], MD, Russ C. Hornbeck[a], MS, Katrina L. Paumier[d], PhD, Prof. Beau M. Ances[d,g], MD, Sarah B. Berman[i], MD, Adam M. Brickman[j,k], PhD, David M. Cash[l,m], PhD, Jasmeer P. Chhatwal[n], MD, Stephen Correia[o], PhD, Stefan Förster[p,q,r], MD, Prof. Nick C. Fox[l], MD, Prof. Neill R. Graff-Radford[s], MD, Prof. Christian la Fougère[r,t], MD, Johannes Levin[q,u], MD, Prof. Colin L. Masters, MD[v], Prof. Martin N. Rossor[l], MD, Prof. Stephen Salloway[o,w], MD, Prof. Andrew J. Saykin[x], PsyD, Prof. Peter R. Schofield[y,z], DSc, Prof. Paul M. Thompson[aa], Ph.D., Prof. Michael M. Weiner[ab], MD, Prof. David M. Holtzman[b,d,g], Prof. Marcus E. Raichle[a,g], MD, Prof. John C. Morris[b,d], MD, Prof. Randall J. Bateman[b,d,g], MD, Tammie L.S. Benzinger[a,b], MD for the Dominantly Inherited Alzheimer Network

[a] Mallinckrodt Institute of Radiology, Washington University in St. Louis, MO, USA
[b] Knight Alzheimer's Disease Research Center, Washington University in St. Louis MO, USA
[c] Division of Biology and Biomedical Sciences, Washington University in St. Louis, MO, USA
[d] Department of Neurology, Washington University in St. Louis, MO, USA
[e] Department of Biostatistics, Washington University in St. Louis, MO, USA
[f] Department of Psychological & Brain Sciences, Washington University in St. Louis, MO, USA
[g] The Hope Center for Neurological Disorders, St. Louis, MO, USA
[h] Department of Radiology, Mayo Clinic and Foundation, Rochester, MN, USA
[i] Department of Neurology, University of Pittsburgh, Pittsburgh, PA, USA (Berman)
[j] Taub Institute for Research on Alzheimer's Disease and the Aging Brain, College of Physicians and Surgeons, Columbia University, New York, NY, USA
[k] Department of Neurology, Columbia University, New York, NY, USA
[l] Dementia Research Centre, Department of Neurodegenerative Disease, University College London Institute of Neurology, London, United Kingdom
[m] Translational Imaging Group, Centre for Medical Image Computing, University College London, London, United Kingdom
[n] Department of Neurology, Massachusetts General Hospital, Harvard Medical School, Boston, USA
[o] Department of Psychiatry, Brown University School of Medicine, Providence, RI, USA
[p] Department of Nuclear Medicine, Technische Universität München, Munich, Germany
[q] German Center for Neurodegenerative Diseases (DZNE) Munich, Germany
[r] German Center for Neurodegenerative Diseases (DZNE) Tübingen, Germany
[s] Department of Neurology, Mayo Clinic, Jacksonville, Florida, USA
[t] Division of Nuclear Medicine and Clinical Molecular Imaging, University Hospital Tübingen, Germany
[u] Department of Neurology, Ludwig-Maximilians-Universität München, Munich, Germany
[v] The Florey Institute, University of Melbourne, Parkville, VIC, Australia
[w] Department of Neurology, Brown University School of Medicine, Providence, RI, USA
[x] Indiana University School of Medicine, Indianapolis, IN, USA
[y] Neuroscience Research Australia, Sydney NSW 2031, Australia
[z] School of Medical Sciences, University of New South Wales, Sydney NSW 2052, Australia
[aa] Imaging Genetics Center, University of Southern California, Marina del Rey, CA, USA
[ab] Department of Radiology and Biomedical Imaging, University of California, San Francisco, CA, USA

* Corresponding Author
[+]Equally contributed to this work

Brian A. Gordon
Email: bagordon@wustl.edu
Phone: 314-747-7354

Author Addresses

Brian A. Gordon bagordon@wustl.edu
Washington University School of Medicine
660 South Euclid, Campus Box 8225
St. Louis, MO 63110

Tyler M. Blazey blazey@wustl.edu
Washington University School of Medicine
660 South Euclid, Campus 8131
St. Louis, MO 63110

Yi Su suy@wustl.edu
Address is the same as TMB

Amrita Hari-Raj amrita.hari-raj@wustl.edu
Address is the same as BAG

Aylin Dincer aylin.dincer@wustl.edu
Address is the same as BAG

Shaney Flores sflores@wustl.edu
Address is the same as BAG

Jon Christensen jonchristensen@wustl.edu
Address is the same as BAG

Eric McDade ericmcdade@wustl.edu
Washington University School of Medicine
660 South Euclid, Campus Box 8111
St. Louis, MO 63110

Guoqiao Wang guoqiao@wustl.edu
Washington University School of Medicine
660 South Euclid, Campus Box 8067
St. Louis, MO 63110

Chengjie Xiong chengjie@wustl.edu
Washington University School of Medicine
660 South Euclid, Campus Box 8067
St. Louis, MO 63110

Nigel J. Cairns cairns@wustl.edu
Washington University School of Medicine
660 South Euclid, Campus Box 8118
St. Louis, MO 63110

Jason Hassenstab hassenstabj@wustl.edu
Knight Alzheimer's Disease Research Center
4488 Forest Park Ave, Suite 301, Campus Box 8111
St. Louis, MO 63108

Daniel S. Marcus dmarcus@wustl.edu
Address is the same as BAG

Anne M. Fagan fagana@neuro.wustl.edu

Washington University School of Medicine
660 South Euclid Ave., Campus Box 8111
St. Louis, MO 63110

Clifford R. Jack Jr. jack.clifford@mayo.edu
Mayo Clinic
200 First Street SW, Rochester,
MN 55905, USA

Russ C. Hornbeck russ@wustl.edu
Address is the same as BAG

Katrina L. Paumier paumierk@wustl.edu
Knight Alzheimer's Disease Research Center
4488 Forest Park Ave, Suite 321, Campus Box 8111
St. Louis, MO 63108

Beau Ances bances@wustl.edu
Washington University School of Medicine
Dept. of Neurology
660 S. Euclid, Box 8111
St. Louis, MO 63110

Sarah B. Berman bermans@upmc.edu
University of Pittsburgh
Biomedical Science Tower 3, 7037
3501 Fifth Avenue
Pittsburgh, PA 15213

Adam M. Brickman amb2139@columbia.edu
Taub Institute for Research on Alzheimer's Disease and the Aging Brain, College of Physicians and
Surgeons, Department of Neurology, Columbia University
630 West 168th Street, P&S Box 16, New York, NY 10032, USA.

David M. Cash d.cash@ucl.ac.uk
Dementia Research Centre
Box 16, National Hospital for Neurology and Neurosurgery
Queen Square
London, WC1N 3BG

Jasmeer P. Chhatwal, chhatwal.jasmeer@mgh.harvard.edu
Massachusetts General Hospital, Dept. of Neurology
Harvard Medical School
149 13th St, Rm 2669
Charlestown, MA 02129

Stephen Correia stephen_correia@brown.edu
Butler Hospital
345 Blackstone Blvd.
Providence, RI 02920

Stefan Förster stefan.foerster@klinikum-bayreuth.de; stefan.foerster@lrz.tum.de
German Center for Neurodegenerative Diseases (DZNE) München and Tübingen &
Dept. of Nuclear Medicine, Technische Universität München (TUM)
Ismaninger Str. 22
81675 Munich

GERMANY

Christian la Fougère Christian.lafougere@med.uni-tuebingen.de
German Center for Neurodegenerative Diseases (DZNE) and Division of Nuclear Medicine and Clinical
Molecular Imaging, University Hospital Tübingen, Germany
Otfried-Müller Str. 14, 72076 Tübingen /Germany

Nick C. Fox n.fox@ucl.ac.uk
Dementia Research Centre
Box 16, National Hospital for Neurology and Neurosurgery
Queen Square
London, WC1N 3BG

Neill R. Graff-Radford MBBCh graffradford.neill@mayo.edu
Mayo Clinic Jacksonville
4500 San Pablo Road
Jacksonville, FL 32224

Johannes Levin Johannes.Levin@med.uni-muenchen.de
Ludwig-Maximilians-Universität München
Klinikum der Universität - Großhadern
Marchioninistraße 15
D-81377 München, Germany

Colin L. Masters c.masters@unimelb.edu.au
The Florey Institute, The University of Melbourne.
Level 5, Kenneth Myer Building
30 Royal Parade
Parkville, Victoria 3010, Australia

Martin Rossor m.rossor@ucl.ac.uk
Dementia Research Centre,
UCL Institute of Neurology
London, WC1N 3BG, United Kingdom

Stephen Salloway SSalloway@Butler.org
The Warren Alpert Medical School of Brown University
345 Blackstone Boulevard
Providence, RI 02906

Andrew J. Saykin asaykin@iupui.edu
Indiana University School of Medicine
355 West 16th Street, Indianapolis, IN 46202

Peter R Schofield p.schofield@neura.edu.au
Neuroscience Research Australia,
Barker Street,
Randwick, Sydney NSW 2031, Australia

Paul M. Thompson pthomp@usc.edu
Imaging Genetics Center, Suite 200
Information Sciences Institute
4676 Admiralty Way
Marina Del Rey, CA 90292

Michael W Weiner Michael.Weiner@ucsf.edu

Veterans Affairs and University of California, San Francisco, CA, USA
4150 Clement St.
San Francisco, CA 94121

David M. Holtzman, holtzman@wustl.edu
Washington University School of Medicine
660 South Euclid, Campus Box 8111
St. Louis, MO 63110

Marcus E. Raichle mraichle@wustl.edu
Address is the same as BAG

John C. Morris jcmorris@wustl.edu
Washington University School of Medicine
4488 Forest Park Avenue, Suite 130, Campus Box 8111
St Louis, Missouri 63108

Randall Bateman batemanr@wustl.edu
Washington University School of Medicine
660 South Euclid, Campus Box 8111
St. Louis, MO 63110

Tammie L.S. Benzinger benzingert@wustl.edu
Address is the same as TMB

Research in context

Evidence before this study
Using PubMed and Google Scholar the authors reviewed prior work on longitudinal neuroimaging markers of Alzheimer pathology with a focus on autosomal dominant Alzheimer disease (ADAD). We searched for all articles prior to October 31st, 2017 with no language restrictions for the keywords Alzheimer's, Alzheimer, longitudinal, positron emission tomography, PET, MRI, atrophy, FDG, hypometabolism, familial, and autosomal. Theories proposed initially in 2010 by Jack and colleagues and revised in 2013 posited temporal trajectories of Alzheimer biomarkers relative to each other and clinical decline. Work by Bateman and colleagues in 2012, Benzinger and colleagues in 2013, and Fleisher and colleagues in 2015 depict such temporal ordering of biomarkers in ADAD populations derived from cross-sectional analyses. There was also a small subset of longitudinal ADAD studies, but these had one or more limitation such as small populations (n<50), examination of only one biomarker, not accounting for regional differences or correlations in the brain, or had a short duration of longitudinal followup.

Added value of this study
Our study presents the first known work examining both the longitudinal temporal trajectories and spatial patterns of Alzheimer pathology in ADAD cohorts using neuroimaging. This work also presents the largest known cohort to date of ADAD individuals studied longitudinally with multiple neuroimaging biomarkers. Longitudinal analyses can provide a more accurate and powerful way to model the temporal emergence of pathology in ADAD. We find that mutation carriers first display Aβ accumulation, followed by hypometabolism, and finally structural atrophy; this is consistent with theoretical models and cross-sectional estimates from ADAD. Most importantly we consider such temporal relationships not in one singular summary measure, but characterize these trajectories throughout the brain. We found that the accrual of pathology varied throughout the brain and by modality in terms of the time of initial emergence and the rates of longitudinal change. These findings suggest region specific vulnerabilities to β-amyloidosis, metabolic decline, and atrophy that change over the course of the disease.

Implications of all the available evidence
Our results build upon existing evidence characterizing biomarkers in clinical and preclinical Alzheimer disease. Our findings suggest that imaging biomarkers follow a sequential pattern, with β-amyloidosis, hypometabolism, and structural atrophy emerging more than twenty, fifteen, and ten years respectively before the expected onset of dementia. Although there is a general hierarchical pattern, there was considerable regional heterogeneity. Most commonly, regions demonstrated an increase in β-amyloidosis and structural atrophy, but there was not evidence of metabolic declines. Further, rather than being homogenous, the same biomarker often demonstrates different longitudinal trajectories across brain regions. Characterizing the temporal and regional dynamics provides insight into disease pathophysiology. This information is critical to decide how to best use neuroimaging biomarkers in clinical trials for subject selection as well as outcomes measures.

Abstract

Background

Models of Alzheimer disease propose a sequence of amyloid-β (Aβ) accumulation, hypometabolism, and structural declines that precede the onset of clinical dementia. These pathological features evolve both temporally and spatially in the brain. This study aimed to characterize where in the brain and when in the course of the disease neuroimaging biomarkers become abnormal.

Methods

We analyzed data from mutation non-carriers, asymptomatic carriers, and symptomatic carriers collected between January 1st 2009 and December 31st 2015 from families carrying *PSEN1*, *PSEN2*, or *APP* mutations enrolled in the Dominantly Inherited Alzheimer's Network. We analyzed [11C]Pittsburgh Compound B positron emission tomography (PiB PET), [18F]Fluorodeoxyglucose (FDG PET), and structural magnetic resonance imaging (MRI) data using regions of interest to assess change throughout the brain. We estimated rates of biomarker change as a function of estimated years from symptom onset at baseline using linear mixed-effects models and determined the earliest point at which biomarker trajectories differed between mutation carriers and non-carriers.

Findings

PiB PET was available for 346 individuals, with 162 having longitudinal imaging; FDG PET was available for 352 (175 longitudinal); and MRI data was available for 377 (201 longitudinal). We found a sequence to pathological changes, with rates of Aβ deposition in mutation carriers being significantly different from non-carriers first (on average across significant regions at -18·9 (sd 3·3) years before expected onset), followed by hypometabolism (-14·1 years, sd 5·1) and lastly structural declines (-4·7 years, sd 4·2). This biomarker ordering was preserved in most, but not all, regions. The temporal emergence within a biomarker varied across the brain, with the precuneus being the first cortical region in each modality to show divergence between groups.

Interpretation

Mutation carriers had elevations in Aβ deposition, reduced glucose metabolism, and cortical thinning which preceded the expected onset of dementia. We found that the accrual of these pathologies varied throughout the brain, suggesting differential regional and temporal vulnerabilities to Aβ, metabolic decline, and structural atrophy. This provides insight into the temporal and spatial development of pathological change in Alzheimer disease. Understanding where and when pathology accrues in the brain is key for using biomarkers in a clinical setting as well as designing and evaluating clinical trials.

Introduction

Alzheimer disease (AD) presents as a progressive loss of cognitive function, leading to severe impairment and loss of independence. AD's long preclinical phase has bolstered efforts to identify *in vivo* biomarkers to aid disease diagnosis and prognosis[1]. Models of AD pathophysiology theorize a temporal sequence where disruptions in amyloid-β (Aβ) production and/or clearance initiate a biological cascade that leads to Aβ plaque formation that spreads throughout the cortex followed by tauopathy, neuronal dysfunction and death, and ultimately dementia[2,3].

Positron emission tomography (PET) and magnetic resonance imaging (MRI) can assess both the amount and location of Aβ plaques, tauopathy (neurofibrillary tangles, neuritic plaques, and neuropil), altered glucose metabolism, and structural decline. The temporal sequence of these biomarkers provides information about the pathogenesis of AD. Determining the ordering of changes in sporadic AD is problematic, as it is difficult to predict an individual's relative position in the disease. Autosomal dominant AD (ADAD) is well suited to study biomarker trajectories due to the virtually complete penetrance of the mutations and consistency of symptom onset within families[4,5]. The conserved onset age within families and mutation types allows individuals to be staged relative to their expected onset of symptoms.

ADAD work has revealed a temporal ordering of biomarkers consistent with theoretical models,[6–8] and indications that pathology progressively appears in new regions of the brain as the disease worsens[7]. This has primarily relied on cross-sectional analyses, with limited analyses of modest longitudinal cohorts[7,9–16]. Longitudinal analyses can provide a better estimate of the true pathological trajectories.[17,18] This is critical as interventional trials such as the Dominantly Inherited Alzheimer Network (DIAN) trials unit,[19] the Alzheimer's Prevention Initiative (API),[20] and the Anti-Amyloid Treatment in Asymptomatic Alzheimer's Study (A4)[21] will all evaluate alterations in longitudinal biomarker trajectories.

The DIAN observational study (DIAN)[4] has established a large cohort of ADAD families

with longitudinal Aβ, metabolic, and structural neuroimaging assessments. Our current work compares rates of biomarker change in a large population of mutation carriers (MC) and non-carriers (NC) throughout the entire brain. In this way we can visualize when pathology biomarkers first emerge and how they spread throughout the course of the disease.

Methods

Participants

Individuals from families known to have mutations in the presenilin 1 (*PSEN1*), presenilin 2 (*PSEN2*), and amyloid precursor protein (*APP*) genes were recruited from 14 performance sites participating in the DIAN observational study (http://www.dian-info.org). Participants were recruited from DIAN sites in the United States, Great Britain, Germany, and Australia between January 1st 2009 and December 31st 2015. All participants with genetic, clinical, and neuroimaging data that passed quality control from the tenth semiannual data freeze were included in the analyses. The institutional review board at Washington University in St. Louis provided supervisory review and human studies approval. Participants or their caregivers provided written informed consent in accordance with their local institutional review board. Clinical and imaging visits in DIAN are performed every three years for asymptomatic individuals until they are within three years of their parental age of dementia onset. Assessments become annual once an individual is within three years of parental age at onset or if an individual becomes symptomatic. Analyses excluded families with the Dutch and Flemish Mutation, as these APP mutations often present with predominant cerebral amyloid angiopathy and diffuse Aβ plaques (see supplemental material). The analyses included 346 individuals with Aβ PET data, 352 with PET metabolism data, and 377 with MRI.

Clinical Assessment.

Dementia status was assessed using the Clinical Dementia Rating (CDR)[22]. For each visit a participant's estimated years from expected symptom onset (EYO) was calculated based upon the participant's current age relative to either the family mutation specific expected age at dementia onset[5] or parental age at first progressive cognitive decline if

mutation age at onset was unknown. A "mutation specific" expected age of dementia onset is calculated by averaging the age of onset reported in the literature across individuals with the same specific mutation[5]. EYO is established identically for both carriers and non-carriers. The presence or absence of an ADAD mutation was determined using PCR-based amplification of the appropriate exon followed by Sanger sequencing[6]. Clinical evaluators were blind to participant mutation status.

MRI.

MRI was performed using the Alzheimer's Disease Neuroimaging Initiative (ADNI) protocol[23]. Sites used a 3T scanner and were required to pass regular quality control assessments. T1-weighted images (1·1 x 1·1 x 1·2-mm voxels) were acquired for all subjects. The ADNI Imaging Core screened images for protocol compliance and artifacts. Volumetric segmentation and cortical surface reconstruction was performed using FreeSurfer 5·3[24,25] which automatically defines subcortical and cortical regions of interest (ROIs). Segmentations were inspected by members of the DIAN Imaging Core and edited as needed. Subcortical volumes were corrected for intracranial volume using a regression approach. Cortical thickness and volume measures were averaged across hemispheres. The cortical and subcortical labels identified on the MRI were utilized for the regional processing of all PET data. For all analyses we examined 34 cortical ROIs and 7 subcortical ROIs. A full list of regions is available in supplemental material.

PET.

Aβ imaging was performed using a bolus injection of [^{11}C]Pittsburgh Compound B (PiB). Acquisition consisted of a 70-minute scan starting at injection or a 30-minute scan beginning 40 minutes post-injection. Data in the common 40–70 minute time frame was converted to regional standardized uptake value ratios (SUVRs) relative to the cerebellar grey matter using FreeSurfer derived regions of interest[26] (PET Unified Pipeline, https://github.com/ysu001/PUP). Metabolic imaging was performed with [^{18}F]Fluorodeoxyglucose (FDG) with a 30-minute dynamic acquisition beginning 30 minutes after injection. Data from the last 20 minutes of each FDG scan were converted to SUVRs relative to cerebellar grey. Both types of PET data were partial volume

corrected using a regional spread function technique[27,28].

As there were no *a priori* laterality predictions, data were averaged across hemispheres before being entered into statistical analyses. Differences in spatial resolution across PET scanners were accounted for by applying scanner specific spatial filters to achieve a common resolution (8 mm)[29]. The ADNI PET Core verified that PET images were acquired using the established protocol and substantially free of artifacts.

Statistical Analyses

We used multivariate linear mixed effects (LME) models to describe the evolution of Alzheimer disease biomarkers. LME models have many benefits including providing a flexible approach to deal with an unequal number of measurement points or intervals. While neuroimaging analyses traditionally use univariate models, the field has begun using multivariate models which account for correlations between regional or voxelwise measurements[30–32]. Multivariate LME models can increased statistical power and reliability compared to univariate methods[30,31]. We implemented a Bayesian multivariate LME model to directly compare longitudinal biomarker changes across brain regions. Cortical and subcortical measurements were analyzed separately for each modality (PiB, FDG, and volumetric), resulting in total of six independent models.

The full Bayesian LME model is described in the supplemental material. Each region included fixed effects for mutation status, time from baseline, baseline EYO, and all possible two and three-way interactions. EYO was modeled as a restricted cubic spline with knots at the 0·10, 0·50, and 0·90 quantiles. We chose restricted cubic splines to model EYO as they represent a flexible approach for accounting for nonlinearities in the data without forcing any particular curve shape. Splines have also been used extensively in the literature to model longitudinal changes in Alzheimer disease biomarkers[33,34]. For every region we included random intercepts and slopes at the subject-level, as well as random intercepts for family affiliation. At the subject-level, covariance matrices were constructed so that intercepts and the slopes were allowed to correlate across all regions in a model.

4

To fit each model we used Stan (http://mc-stan.org/)[35,36], an open source package for Hamilton Markov chain Monte Carlo analyses. A parameter, or combination of parameters, was considered statistically significant if the 99% equal-tailed credible intervals of the posterior distribution did not overlap zero. Analyses were run separately for each modality (MRI, PiB, and FDG). Within each modality one model simultaneously fit 34 cortical ROIs and a second model simultaneously fit 7 subcortical ROIs derived from FreeSurfer. Each regional comparison within a model is simply a different slice of the same multidimensional posterior distribution. The current analyses focus on the interaction between mutation status and the longitudinal rate of change. Including multiple regions within one model also allows for the direct comparison of rates of changes between regions (supplemental material).

Role of the funding source

The study sponsors had no role in the study design, data collection, data analysis, data interpretation, writing of the report, or the decision to submit the manuscript for publication. All coauthors had full access to the data in the study and the corresponding author had final responsibility for the decision to submit for publication.

Results

Population demographics are in Table 1. Subjects with longitudinal data had an average of 2·4 visits (sd 0·8) and 2·7 (sd 1·1) years of data. Figure 1 shows example LME model fits for one region. For the both the middle and right-hand panels the shaded areas represent 99% credible intervals around the model estimates. The credible intervals are drawn from the actual distributions of model fits derived by the Hamilton Markov Chain Monte Carlos analyses. Any point in the difference curves (right-hand panels) where the shaded area is not touching the zero axis is a point in the disease progression (as measured by EYO) where the biomarker rate of change is different between groups. The first EYO point that was significantly different between groups was considered the initial diverge between groups. Figures depicting the model results for every ROI are available in supplemental materials. To avoid inadvertently revealing participants' mutation status

at the edges of our sample where there are only a few individuals, figures are displayed with baseline EYO -29 to +10.

The rate of Aβ accumulation is statistically higher in MC relative to NC participants starting more than two decades (EYO -22·2) before the expected age of dementia onset (Figure 1). As glucose utilization represents a natural biological property it contains both maturational and disease-related trajectories. In both groups, the precuneus FDG trajectories were initially positive, became neutral, and then negative. This negative directional acceleration begins earlier and was larger in MCs, with the rate of change becoming significantly less than NC at EYO -18·8. Finally, precuneus cortical thinning significantly differs in MC relative to NC at EYO -13·0. Supplemental material contains results for every ROI. Overall, in regions with a significant effect relative to NC, rates of Aβ deposition were significantly higher in MC at an average EYO of -18·9 (sd 3·3), metabolism began declining at an average EYO of -14·1 (sd 5·1), and MRI structural measures declined at an average EYO -4·7 (sd 4·2).

Figure 2 depicts EYOs when and whether the longitudinal rate of change first differs between MC and NC for each biomarker. The differences across regions and modalities reflect the temporal and spatial evolution of pathology over the course of the disease. Rates of biomarkers change in regions that are grey are never significantly different between groups. This information is presented in numeric form in Supplemental Tables 1 and 2. While many regions follow trajectories similar to the precuneus, the emergence of pathology varied throughout the brain. Further, there were regional differences by modality, for example, relative to NC the superior temporal lobe did not demonstrate a metabolic loss, but had atrophy changes at -5·6 EYO. Figure 3 depicts rates of change in MC for three cortical and three subcortical regions that exemplify common patterns.

For PiB PET, 32/34 cortical regions showed significantly greater longitudinal rates of accumulation in MC relative to NC. The first point of divergence between groups varied across regions (EYO -22·2 to -2·5), with the precuneus, posterior cingulate gyrus, and medial orbital frontal cortex regions showing the earliest changes (~EYO -21). Of the 32

regions with significant differences, all but the cuneus (-2·5) occurred prior to an EYO of -15. In the seven subcortical regions the accumbens (-22·2), putamen (-17·0), and caudate (-16·4) demonstrated greater PiB accumulation rates in MC while the amygdala, hippocampus, palladium, and thalamus did not differ. Significant differences in progressive hypometabolism in MC relative to NC were less pronounced, with 8/34 cortical regions demonstrating significant interactions. The effects ranged from EYO -18·8 to -2·8, with the earliest effects detected in the precuneus, banks of the superior temporal sulcus, and caudal middle frontal cortex (EYO ~-18). No subcortical regions showed significant differences in the rate of FDG change. For MRI 24/34 cortical and 4/7 subcortical areas demonstrated increased rates of atrophy in MC relative to NC with effects appearing from EYO -13·0 to 2·3. The precuneus (-13·0), banks of the superior temporal sulcus (-11·5), and inferior parietal cortex (-10·6) demonstrated the earliest changes.

We also observed regional differences in the rates of biomarker change within the MC group. In the precuneus there was a rapid increase in Aβ deposition; this rate peaked but remained positive even after the predicted onset of dementia (Figure 3 and Figure 4). This was the most common pattern across areas. In other regions (e.g. insula) initial accelerations in Aβ deposition were followed by decelerations, leading to a plateau of total Aβ levels. In a subset of regions (e.g. inferior temporal cortex) the estimated rate of Aβ accumulation accelerates throughout the disease. Once declining, glucose metabolism in the precuneus showed prominent, worsening rates of hypometabolism before the rates stabilized (~ EYO -5), while in inferior temporal cortex the rate of metabolic loss modestly increased initially before quickly plateauing (Figure 3B). Many regions had relatively small rates of metabolic decline in MC, even at later EYOs. In regions with structural decline the trajectories were fairly consistent, with the rate of atrophy accelerating as the disease progressed. However, the absolute rate of decline was often different between regions. Matrices directly comparing the regional rates of change for each biomarker at different EYOs (-25, -15, -5, and 5) can be found in supplemental material. Voxel-wise movies depict the rate of change and total biomarker levels in MC at every EYO and the creation of these movies is detailed in supplemental material.

7

Discussion

AD is not static but possesses dynamism in terms of what pathological processes first appear, and how such pathology propagates throughout the brain. As dementia onset is predictable in ADAD, it provides an elegant model with which to examine pathological staging. Characterizing the spatial and temporal spread of pathology provides insight to the pathophysiology of the disease, informs how neuroimaging could aid optimal subject recruitment in clinical trials, and is critical to measure the efficacy of interventions on longitudinal biomarker measurements.

The primary goal of the current analysis was to find the first biomarker time point in the course of the disease where carriers of ADAD mutations demonstrated different rates of pathological progression relative-to non-carrier family members. This time point can be interpreted as the moment where longitudinal change in that brain area due to AD can first be detected with *in vivo* neuroimaging. The primary questions using this approach focused on regional differences across the brain within a marker (e.g. precuneus vs. parietal Aβ PET) as well as comparing spatial differences between biomarkers (e.g. Aβ PET vs. FDG PET).

Consistent with prior work we found that Aβ deposition was the first biomarker to demonstrate differences between mutation groups. MC had greater Aβ deposition more than 20 years before the expected age of symptom onset. Aβ increases were near ubiquitous, with most regions changing more than 14 years before the expected year of dementia. Measures of metabolism in ADAD represent overlapping maturational and disease changes. Both NC and MC cohorts had inverted U-shaped trajectories (Figure 1D & 1E), with the absolute levels of glucose metabolism initially modestly increasing with EYO, followed by a prolonged decrease. The key difference is that MC showed metabolic reductions earlier and to a greater degree than NC. While cross-sectional values still overlapped between groups early in the disease, longitudinal trajectories reveal divergence (supplementary material). The precuneus demonstrates the earliest metabolic decrease an EYO of -18·8, with significant regions on average becoming

abnormal at EYO -14·1. Reductions in grey matter were the last neuroimaging biomarker to manifest and occured over the majority of the brain. Again the precuneus is one of the earliest regions to change, with declines emerging a decade before estimated dementia onset, while overall declines were most prolific in the five years preceding expected dementia onset. The direct comparison of the rates of biomarker change between regions is presented in supplementary material.

The relationships between the three biomarkers are complex. While all regions with metabolic decreases have abnormal Aβ accumulation, many regions with abnormal Aβ accumulation rates did not demonstrate elevated metabolic decline. Although FDG hypometabolism and structural decline are markers of degeneration, our results indicate they can be incongruent. In regions where they both occur, declines in glucose metabolism precede atrophy by ~5 to 10 years. However, there are regions that demonstrated β-amyloidosis and structural atrophy where significant metabolic decline was not detected (e.g. occipital and temporal regions). Portions of the medial temporal lobe (e.g. the hippocampus) did not manifest pathological change in Aβ or FDG, but had structural declines. Although there is generally a tripartite hierarchy such that β-amyloidosis precedes metabolic decline that in turn precede atrophy, these relationships are highly heterogeneous across the cortex.

Discordance between imaging biomarkers has been noted in sporadic AD [37–44]. Due to the cross-sectional nature of the majority of the work, such spatial incongruences could be due to temporal lags in the emergence of pathologies.[42,44] EYO, as a marker of disease time, is perfectly suited to detect such temporal evolutions. The current work does indeed clearly demonstrate that a temporal progression is present in some regions (e.g. PiB, FDG, and cortical thinning in the precuneus). However, despite the long disease window covered by the current study population, some region still only demonstrate a subset of pathologies. This suggests the incongruences are not simply a product of temporal lag, but can represent true heterogeneity. Other, unobserved, biomarkers such as those that measure tau pathology and inflammation, may help explain this heterogeneous relationship.

The current work presents the largest and most comprehensive analysis of neuroimaging data in ADAD to date. Still, the majority of longitudinal subjects had only a limited follow-up (average 2·4 visits); results at the edges of the EYO range where outliers have disproportional influence must be interpreted with care. There are also only modest numbers of subjects with PSEN2 and APP mutations. As the DIAN study gains more time points longitudinal estimates will be improved further and it may be possible to compare the three types of mutations. A greater number of individuals and time points will also increase the feasibility of modeling multiple modalities simultaneously across all brain regions as previously done using summary measures of pathology.[45]

The temporal and spatial ordering of biomarkers must also be interpreted with caveats. No one individual has data across the entire disease window, and our results represent population rather than individual subject effects. Further, as seen in regional fits (Figure 1 and supplemental material) some individuals differ from population trajectories. Thus, imaging data alone may not be sufficient to make individual-level disease stage predictions. Such predictions would require further work that accounts for individual differences due to factors such as genetic variability and lifestyle. The current work also utilizes partial volume corrected PET data,[27,28] analyses without this step could have slightly different trajectories late in the disease.

The temporal ordering of biomarker change must also be viewed as relative rather than absolute. Our models are fit using a particular definition of EYO. Supplemental models using a modified definition of EYO indicate a preserved relative ordering (e.g. precuneus Aβ > hypometabolism > structural decline) but slight differences in absolute timing (e.g. shifts from EYO -22·2 to -19·8). Further, our results reflect the first *detectable* changes with PET and MRI, which are constrained by the inherent sensitivities and signal to noise properties of the imaging techniques. The current analyses utilize the cerebellum as a reference region for PET. Results using the brainstem instead were essentially unchanged (Supplementary Tables 3 and 4). Finally, although ADAD can serve as a model for sporadic AD, direct comparisons must explore potential differences.

Our results reveal complex patterns of biomarker accumulation across the brain. Elevations in β-amyloidosis occur more than two decades before and continue to accrue even after the expected year of symptom onset. Neurodegeneration measured with both FDG and structural MRI begins while Aβ is still increasing and occurs closer in time, but still well before the onset of dementia. While global measures likely capture a large degree of intraindividual variability, our results indicate not just when, but where pathology emerges in the brain. Understanding such longitudinal change provides insight into the pathophysiological progression of AD and has implications for clinical trials.

Contributors

BAG and TMB equally contributed to the present work and wrote the manuscript, analyzed the data, and generated the figures and movies. YS, AH, AD, SF, JC, CRJ, and MMW oversaw data quality control and processing. CX, NJC, JH, DSM, AMF, DMH, RCH, KLP, EM, GW, MER, JCM, RJB, and TLSB and oversaw overall study design and general implementation. RJB and TLSB assisted in data interpretation. BMA, SBB, AMB, DMC, JPC, SC, StF, NCF, NRG, CF, JL, CLM, MNR, SS, AJS, PRS, and PMT oversaw study implementation and data collection at their respective institutions. All authors revised the manuscript.

Declarations of Interest

BAG and BMA report participating in a clinical trial of AV-1451 sponsored by Avid Radiopharmaceuticals. EM reports grants from Dominantly Inherited Alzheimer Network Trials Unit Pharma Consortium, outside the submitted work. CX reports grants from the NIA outside the submitted work. JH reports personal fees from Biogen and Lundbeck, outside the submitted work. CRJ reports consulting services for Lilly Co. and grants from NIH, outside the submitted work. DSM reports grants from the NIH outside and support from Radiologics, Inc., both outside the conduct of the study. AMF reports personal fees from DiamiR, personal fees from LabCorp, personal fees from IBL International, personal fees from Genentech, grants from Roche Diagnostics, grants from Fujirebio, grants from Biogen, outside the submitted work. DMC reports grants from Alzheimer's

Acknowledgements

Figure 1: Modeling longitudinal change in the precuneus for PiB (top), FDG (middle), and cortical thickness (bottom). The left-hand panels (A, D, & G) depict the model estimates of longitudinal biomarkers. The middle panels (B, E, & H) depict the estimated rate of change across the course of the disease for mutation carriers and non-carriers. Individual random effect slope estimates are plotted as colored dots. The right hand panels (C, F, and I) depict the difference in rate of biomarker change between mutation carriers and non-carriers across the course of the disease. For both the middle and right-hand panels the shaded areas represent 99% credible intervals around the model estimates. Any point in this difference curves where the shaded area is not touching the zero axis is a point in the disease progression (as measured by EYO) where the biomarker accumulation rate is different between groups. Figures depicting the model results for every ROI are available in supplemental materials. To avoid inadvertently revealing mutation status figures are displayed with baseline EYO -29 to +10.

Figure 2: Emergence of neuroimaging biomarkers. The color scale represents the first point in the disease relative to estimated age at onset (EYO) where rates of biomarker change in that cortical region are significantly different between mutation carriers and non-carriers (akin to the first point where credible interval are different from zero in Figure 1 right panels). There is a temporal evolution where increased Aβ deposition precedes hypometabolism that in turn is followed by cortical thinning. Information for all modalities and regions is presented in numeric form in Supplemental Tables 1 and 2.

Figure 3: Trajectories of biomarker accumulation in mutation carriers for three cortical (top) and three subcortical regions (bottom) for PiB (left), FDG (middle), and structural MRI (right) that highlight different patterns of change seen in different brain regions.

Figure 4: Depictions of model estimates of rate of change in PiB (top), FDG (middle), and cortical thickness (bottom) in mutation carriers at an EYO of -25, -15, -5, and +5.

Table 1: Study demographics at baseline.

Demographics at Baseline			
	Non-Carriers	Asymptomatic Carriers	Symptomatic Carriers
Number	148	141	88
Females (%)	85 (57%)	78 (55%)	49 (56%)
Age (years/sd)	39·5 (11·4)	34·6 (9·2)	45·7 (9·9)
MMSE (mean/sd)	29·0 (2·7)	28·8 (2·7)	23·9 (10·2)
CDR-SOB (mean/SD)	0·0 (0·2)	0·0 (0·1)	3·6 (3·5)
EYO (years/sd)	-8·9 (11·4)	-13·7 (9·2)	0·5 (7·1)
PSEN1/PSEN2/APP	122/17/9	117/16/8	76/6/6
	(82/11/6%)	(83/11/6%)	(86/7/7%)
N with Follow up (%)	70 (47%)	73 (52%)	58 (66%)
N of visits*(sd)	2·3 (0·8)	2·3 (0·8)	2·8 (1·2)
Follow up in years* (sd)	3·0 (1·7)	3·0 (1·6)	2·0 (1·3)

Summary of Imaging Data			
Data By Modality	PIB	FDG	MRI
1 visit	184	177	176
2 visits	124	131	145
3 visits	23	27	35
4 visits	10	11	11
5 visits	4	5	8
6 visits	1	1	2
Total Subjects	346	352	377

*Summary values are only for those individuals with longitudinal data

EYO - estimated years to dementia onset

MMSE –Mini Mental State Examination

CDR-SOB – Clinical Dementia Rating Sum of Boxes

References

1   Pike KE, Savage G, Villemagne VL, *et al.* β-amyloid imaging and memory in non-demented individuals: evidence for preclinical Alzheimer's disease. *Brain* 2007; **130**.

2   Hardy JA, Higgins GA. Alzheimer's disease: The amyloid cascade hypothesis. Science (80-.). 1992; **256**: 184–5.

3   Jack CR, Knopman DS, Jagust WJ, *et al.* Tracking pathophysiological processes in Alzheimer's disease: an updated hypothetical model of dynamic biomarkers. *Lancet Neurol* 2013; **12**: 207–16.

4   Moulder KL, Snider BJ, Mills SL, *et al.* Dominantly Inherited Alzheimer Network: facilitating research and clinical trials. *Alzheimers Res Ther* 2013; **5**: 48.

5   Ryman DC, Acosta-Baena N, Aisen PS, *et al.* Symptom onset in autosomal dominant Alzheimer disease: a systematic review and meta-analysis. *Neurology* 2014; **83**: 253–60.

6   Bateman RJ, Xiong C, Benzinger TLS, *et al.* Clinical and biomarker changes in dominantly inherited Alzheimer's disease. *N Engl J Med* 2012; **367**: 795–804.

7   Benzinger TLS, Blazey T, Jack CR, *et al.* Regional variability of imaging biomarkers in autosomal dominant Alzheimer's disease. *Proc Natl Acad Sci U S A* 2013; **110**: E4502-4509.

8   Fleisher AS, Chen K, Quiroz YT, *et al.* Associations between biomarkers and age in the presenilin 1 E280A autosomal dominant Alzheimer disease kindred: a cross-sectional study. *JAMA Neurol* 2015; **72**: 316–24.

9   Yau W-YW, Tudorascu DL, McDade EM, *et al.* Longitudinal assessment of neuroimaging and clinical markers in autosomal dominant Alzheimer's disease: a prospective cohort study. *Lancet Neurol* 2015; **14**: 804–13.

10   Weston PSJ, Nicholas JM, Lehmann M, *et al.* Presymptomatic cortical thinning in familial Alzheimer disease: A longitudinal MRI study. *Neurology* 2016; : 10.1212/WNL.0000000000003322.

11   Wang F, Gordon BA, Ryman DC, *et al.* Cerebral amyloidosis associated with cognitive decline in autosomal dominant Alzheimer disease. *Neurology* 2015; published online Aug 5. DOI:10.1212/WNL.0000000000001903.

12   Sala-Llonch R, Llad? A, Fortea J, *et al.* Evolving brain structural changes in PSEN1 mutation carriers. *Neurobiol Aging* 2015; **36**: 1261–70.

13   Schott JM, Fox NC, Frost C, *et al.* Assessing the onset of structural change in familial Alzheimer's disease. *Ann Neurol* 2003; **53**: 181–8.

14   Fagan AM, Xiong C, Jasielec MS, *et al.* Longitudinal change in CSF biomarkers in autosomal-dominant Alzheimer's disease. *Sci Transl Med* 2014; **6**: 226ra30.

15   Knight WD, Kim LG, Douiri A, Frost C, Rossor MN, Fox NC. Acceleration of cortical thinning in familial Alzheimer's disease. *Neurobiol Aging* 2011; **32**: 1765–73.

16   Kinnunen KM, Cash DM, Poole T, *et al.* Presymptomatic atrophy in autosomal dominant Alzheimer's disease: a serial MRI study. *Alzheimer's Dement*.

17   Thompson WK, Hallmayer J, O'Hara R, Initiative the ADN. Design Considerations for Characterizing Psychiatric Trajectories Across the Lifespan: Application to Effects of APOE-ε4 on Cerebral Cortical Thickness in Alzheimer's

Disease. *Am J Psychiatry* 2011; **168**: 894–903.

18   Xu Z, Shen X, Pan W, *et al.* Longitudinal analysis is more powerful than cross-sectional analysis in detecting genetic association with neuroimaging phenotypes. *PLoS One* 2014; **9**: e102312.

19   Mills SM, Mallmann J, Santacruz AM, *et al.* Preclinical trials in autosomal dominant AD: implementation of the DIAN-TU trial. *Rev Neurol (Paris)* 2013; **169**: 737–43.

20   Reiman EM, Langbaum JBS, Fleisher AS, *et al.* Alzheimer's Prevention Initiative: a plan to accelerate the evaluation of presymptomatic treatments. *J Alzheimers Dis* 2011; **26 Suppl 3**: 321–9.

21   Sperling R a A, Rentz DMM, Johnson K a A, *et al.* The A4 Study: Stopping AD before Symptoms Begin? *Sci Transl Med Med* 2014; **6**: 228fs13-228fs13.

22   Morris JC. The Clinical Dementia Rating (CDR): Current version and scoring rules. *Neurology* 1993; **43**: 2412–4.

23   Jack CCR, Bernstein MA, Borowski BBJ, *et al.* Update on the magnetic resonance imaging core of the Alzheimer's disease neuroimaging initiative. *Alzheimer's Dement* 2010; **6**: 212–20.

24   Fischl B. FreeSurfer. *Neuroimage* 2012; **62**: 774–81.

25   Fischl B, Dale AMM. Measuring the thickness of the human cerebral cortex from magnetic resonance images. *Proc Natl Acad Sci U S A* 2000; **97**: 11050–5.

26   Su Y, D'Angelo GM, Vlassenko AG, *et al.* Quantitative Analysis of PiB-PET with FreeSurfer ROIs. *PLoS One* 2013; **8**: e73377.

27   Su Y, Blazey TM, Snyder AZ, *et al.* Partial volume correction in quantitative amyloid imaging. *Neuroimage* 2015; **107**: 55–64.

28   Rousset OG, Ma Y, Evans AC. Correction for partial volume effects in PET: Principle and validation. *J Nucl Med* 1998; **39**: 904–11.

29   Joshi A, Koeppe RA, Fessler JA. Reducing between scanner differences in multi-center PET studies. *Neuroimage* 2009; **46**: 154–9.

30   Bernal-Rusiel JL, Reuter M, Greve DN, Fischl B, Sabuncu MR. Spatiotemporal linear mixed effects modeling for the mass-univariate analysis of longitudinal neuroimage data. *Neuroimage* 2013; **81**: 358–70.

31   Bernal-Rusiel JL, Greve DN, Reuter M, Fischl B, Sabuncu MR. Statistical analysis of longitudinal neuroimage data with Linear Mixed Effects models. *Neuroimage* 2013; **66**: 249–60.

32   Bilgel M, Prince JL, Wong DF, Resnick SM, Jedynak BM. A multivariate nonlinear mixed effects model for longitudinal image analysis: Application to amyloid imaging. *Neuroimage* 2016; **134**: 658–70.

33   Jack CR, Wiste HJ, Lesnick TG, *et al.* Brain β-amyloid load approaches a plateau. *Neurology* 2013; **80**: 890–6.

34   Jack CR, Vemuri P, Wiste HJ, *et al.* Shapes of the trajectories of 5 major biomarkers of Alzheimer disease. *Arch Neurol* 2012; **69**: 856–67.

35   Carpenter B, Lee D, Brubaker MA, *et al.* Stan: A Probabilistic Programming Language. *J Stat Softw* 2016.

36   Gelman A, Lee D, Guo J. Stan: A Probabilistic Programming Language for Bayesian Inference and Optimization. *J Educ Behav Stat* 2015; **40**: 530–43.

37   Gordon BA, Blazey T, Benzinger TL. Regional variability in Alzheimer's disease

biomarkers. *Future Neurol* 2014; **9**: 131–4.

38 La Joie R, Perrotin A, Barré L, *et al.* Region-specific hierachy between atrophy, hypometabolism, and β-amyloid (Aβ) load in Alzheimer's disease dementia. *J Neurosci* 2012; **32**: 16265–73.

39 Grothe MJ, Teipel SJ. Spatial patterns of atrophy, hypometabolism, and amyloid deposition in Alzheimer's disease correspond to dissociable functional brain networks. *Hum Brain Mapp* 2016; **37**: 35–53.

40 Edison P, Archer HA, Hinz R, *et al.* Amyloid, hypometabolism, and cognition in Alzheimer disease: an [11C]PIB and [18F]FDG PET study. *Neurology* 2007; **68**: 501–8.

41 Lehmann M, Ghosh PM, Madison C, *et al.* Diverging patterns of amyloid deposition and hypometabolism in clinical variants of probable Alzheimer's disease. *Brain* 2013; **136**: 844–58.

42 Förster S, Grimmer T, Miederer I, *et al.* Regional Expansion of Hypometabolism in Alzheimer's Disease Follows Amyloid Deposition with Temporal Delay. *Biol Psychiatry* 2012; **71**: 792–7.

43 Alexopoulos P, Kriett L, Haller B, *et al.* Limited agreement between biomarkers of neuronal injury at different stages of Alzheimer's disease. *Alzheimer's Dement* 2014; **10**: 684–9.

44 Förster S, Yousefi BH, Wester H-J, *et al.* Quantitative longitudinal interrelationships between brain metabolism and amyloid deposition during a 2-year follow-up in patients with early Alzheimer's disease. *Eur J Nucl Med Mol Imaging* 2012; **39**: 1927–36.

45 Donohue MC, Jacqmin-Gadda H, Le Goff M, *et al.* Estimating long-term multivariate progression from short-term data. *Alzheimer's Dement* 2014; **10**: S400–10.

*Manuscript with revisions highlighted

Spatial patterns of ~~longitudinal~~ neuroimaging biomarker change in <u>individuals from families with</u> autosomal dominant Alzheimer disease<u>: a longitudinal study</u>

Brian A. Gordon*[+][a,b], PhD, Tyler M. Blazey[+][a,c], BS, Yi Su[a], PhD, Amrita Hari-Raj[a], BA, Aylin Dincer[a], BA, Shaney Flores[a], BS, Jon Christensen[a], BS, Eric McDade[c,d], DO, Guoqiao Wang[d], PhD, <u>Prof.</u> Chengjie Xiong[b,e], PhD, <u>Prof.</u> Nigel J. Cairns[b,d], PhD, Jason Hassenstab[b,d,f], PhD, Daniel S. Marcus[a], PhD, <u>Prof.</u> Anne M. Fagan[b,d,g], PhD[d], <u>Prof.</u> Clifford R. Jack Jr.[h], MD, Russ C. Hornbeck[a], MS, Katrina L. Paumier[d], PhD, <u>Prof.</u> Beau M. Ances[d,g], MD, Sarah B. Berman[i], MD, Adam M. Brickman[j,k], <u>PhD</u>, David M. Cash[l,m], PhD, Jasmeer P. Chhatwal[n], MD, Stephen Correia[o], PhD, Stefan Förster[p,q,r], MD, <u>Prof.</u> Nick C. Fox[l], MD, <u>Prof.</u> Neill R. Graff-Radford[s], MD, <u>Prof.</u> Christian la Fougère[r,t], MD, Johannes Levin[q,u], MD, <u>Prof.</u> Colin L. Masters, MD[v], <u>Prof.</u> Martin N. Rossor[l], MD, <u>Prof.</u> Stephen Salloway[o,w], MD, <u>Prof.</u> Andrew J. Saykin[x], PsyD, <u>Prof.</u> Peter R. Schofield[y,z], DSc, <u>Prof.</u> Paul M. Thompson[aa], Ph.D., <u>Prof.</u> Michael M. Weiner[ab], MD, <u>Prof.</u> David M. Holtzman[b,d,g], <u>Prof.</u> Marcus E. Raichle[a,g], MD, <u>Prof.</u> John C. Morris[b,d], MD, <u>Prof.</u> Randall J. Bateman[b,d,g], MD, Tammie L.S. Benzinger[a,b], MD for the Dominantly Inherited Alzheimer Network

[a] Mallinckrodt Institute of Radiology, Washington University in St. Louis, MO, USA
[b] Knight Alzheimer's Disease Research Center, Washington University in St. Louis MO, USA
[c] Division of Biology and Biomedical Sciences, Washington University in St. Louis, MO, USA
[d] Department of Neurology, Washington University in St. Louis, MO, USA
[e] Department of Biostatistics, Washington University in St. Louis, MO, USA
[f] Department of Psychological & Brain Sciences, Washington University in St. Louis, MO, USA
[g] The Hope Center for Neurological Disorders, St. Louis, MO, USA
[h] Department of Radiology, Mayo Clinic and Foundation, Rochester, MN, USA
[i] Department of Neurology, University of Pittsburgh, Pittsburgh, PA, USA (Berman)
[j] Taub Institute for Research on Alzheimer's Disease and the Aging Brain, College of Physicians and Surgeons, Columbia University, New York, NY, USA
[k] Department of Neurology, Columbia University, New York, NY, USA
[l] Dementia Research Centre, Department of Neurodegenerative Disease, University College London Institute of Neurology, London, United Kingdom
[m] Translational Imaging Group, Centre for Medical Image Computing, University College London, London, United Kingdom
[n] Department of Neurology, Massachusetts General Hospital, Harvard Medical School, Boston, USA
[o] Department of Psychiatry, Brown University School of Medicine, Providence, RI, USA
[p] Department of Nuclear Medicine, Technische Universität München, Munich, Germany
[q] German Center for Neurodegenerative Diseases (DZNE) Munich, Germany
[r] German Center for Neurodegenerative Diseases (DZNE) Tübingen, Germany
[s] Department of Neurology, Mayo Clinic, Jacksonville, Florida, USA
[t] Division of Nuclear Medicine and Clinical Molecular Imaging, University Hospital Tübingen, Germany
[u] Department of Neurology, Ludwig-Maximilians-Universität München, Munich, Germany
[v] The Florey Institute, University of Melbourne, Parkville, VIC, Australia
[w] Department of Neurology, Brown University School of Medicine, Providence, RI, USA
[x] Indiana University School of Medicine, Indianapolis, IN, USA
[y] Neuroscience Research Australia, Sydney NSW 2031, Australia
[z] School of Medical Sciences, University of New South Wales, Sydney NSW 2052, Australia
[aa] Imaging Genetics Center, University of Southern California, Marina del Rey, CA, USA
[ab] Department of Radiology and Biomedical Imaging, University of California, San Francisco, CA, USA

* Corresponding Author
[+] Equally contributed to this work

Brian A. Gordon
Email: bagordon@wustl.edu
Phone: 314-747-7354

Author Addresses

Brian A. Gordon bagordon@wustl.edu
Washington University School of Medicine
660 South Euclid, Campus Box 8225
St. Louis, MO 63110

Tyler M. Blazey blazey@wustl.edu
Washington University School of Medicine
660 South Euclid, Campus 8131
St. Louis, MO 63110

Yi Su suy@wustl.edu
Address is the same as TMB

Amrita Hari-Raj amrita.hari-raj@wustl.edu
Address is the same as BAG

Aylin Dincer aylin.dincer@wustl.edu
Address is the same as BAG

Shaney Flores sflores@wustl.edu
Address is the same as BAG

Jon Christensen jonchristensen@wustl.edu
Address is the same as BAG

Eric McDade ericmcdade@wustl.edu
Washington University School of Medicine
660 South Euclid, Campus Box 8111
St. Louis, MO 63110

Guoqiao Wang guoqiao@wustl.edu
Washington University School of Medicine
660 South Euclid, Campus Box 8067
St. Louis, MO 63110

Chengjie Xiong chengjie@wustl.edu
Washington University School of Medicine
660 South Euclid, Campus Box 8067
St. Louis, MO 63110

Nigel J. Cairns cairns@wustl.edu
Washington University School of Medicine
660 South Euclid, Campus Box 8118
St. Louis, MO 63110

Jason Hassenstab hassenstabj@wustl.edu
Knight Alzheimer's Disease Research Center
4488 Forest Park Ave, Suite 301, Campus Box 8111
St. Louis, MO 63108

Daniel S. Marcus dmarcus@wustl.edu
Address is the same as BAG

Anne M. Fagan fagana@neuro.wustl.edu

Washington University School of Medicine
660 South Euclid Ave., Campus Box 8111
St. Louis, MO 63110

Clifford R. Jack Jr. jack.clifford@mayo.edu
Mayo Clinic
200 First Street SW, Rochester,
MN 55905, USA

Russ C. Hornbeck russ@wustl.edu
Address is the same as BAG

Katrina L. Paumier paumierk@wustl.edu
Knight Alzheimer's Disease Research Center
4488 Forest Park Ave, Suite 321, Campus Box 8111
St. Louis, MO 63108

Beau Ances bances@wustl.edu
Washington University School of Medicine
Dept. of Neurology
660 S. Euclid, Box 8111
St. Louis, MO 63110

Sarah B. Berman bermans@upmc.edu
University of Pittsburgh
Biomedical Science Tower 3, 7037
3501 Fifth Avenue
Pittsburgh, PA 15213

Adam M. Brickman amb2139@columbia.edu
Taub Institute for Research on Alzheimer's Disease and the Aging Brain, College of Physicians and
Surgeons, Department of Neurology, Columbia University
630 West 168th Street, P&S Box 16, New York, NY 10032, USA.

David M. Cash d.cash@ucl.ac.uk
Dementia Research Centre
Box 16, National Hospital for Neurology and Neurosurgery
Queen Square
London, WC1N 3BG

Jasmeer P. Chhatwal, chhatwal.jasmeer@mgh.harvard.edu
Massachusetts General Hospital, Dept. of Neurology
Harvard Medical School
149 13th St, Rm 2669
Charlestown, MA 02129

Stephen Correia stephen_correia@brown.edu
Butler Hospital
345 Blackstone Blvd.
Providence, RI 02920

Stefan Förster stefan.foerster@klinikum-bayreuth.de; stefan.foerster@lrz.tum.de
German Center for Neurodegenerative Diseases (DZNE) München and Tübingen &
Dept. of Nuclear Medicine, Technische Universität München (TUM)
Ismaninger Str. 22
81675 Munich

GERMANY

Christian la Fougère Christian.lafougere@med.uni-tuebingen.de
German Center for Neurodegenerative Diseases (DZNE) and Division of Nuclear Medicine and Clinical
Molecular Imaging, University Hospital Tübingen, Germany
Otfried-Müller Str. 14, 72076 Tübingen /Germany

Nick C. Fox n.fox@ucl.ac.uk
Dementia Research Centre
Box 16, National Hospital for Neurology and Neurosurgery
Queen Square
London, WC1N 3BG

Neill R. Graff-Radford MBBCh graffradford.neill@mayo.edu
Mayo Clinic Jacksonville
4500 San Pablo Road
Jacksonville, FL 32224

Johannes Levin Johannes.Levin@med.uni-muenchen.de
Ludwig-Maximilians-Universität München
Klinikum der Universität - Großhadern
Marchioninistraße 15
D-81377 München, Germany

Colin L. Masters c.masters@unimelb.edu.au
The Florey Institute, The University of Melbourne.
Level 5, Kenneth Myer Building
30 Royal Parade
Parkville, Victoria 3010, Australia

Martin Rossor m.rossor@ucl.ac.uk
Dementia Research Centre,
UCL Institute of Neurology
London, WC1N 3BG, United Kingdom

Stephen Salloway SSalloway@Butler.org
The Warren Alpert Medical School of Brown University
345 Blackstone Boulevard
Providence, RI 02906

Andrew J. Saykin asaykin@iupui.edu
Indiana University School of Medicine
355 West 16th Street, Indianapolis, IN 46202

Peter R Schofield p.schofield@neura.edu.au
Neuroscience Research Australia,
Barker Street,
Randwick, Sydney NSW 2031, Australia

Paul M. Thompson pthomp@usc.edu
Imaging Genetics Center, Suite 200
Information Sciences Institute
4676 Admiralty Way
Marina Del Rey, CA 90292

Michael W Weiner Michael.Weiner@ucsf.edu

Veterans Affairs and University of California, San Francisco, CA, USA
4150 Clement St.
San Francisco, CA 94121

David M. Holtzman, holtzman@wustl.edu
Washington University School of Medicine
660 South Euclid, Campus Box 8111
St. Louis, MO 63110

Marcus E. Raichle mraichle@wustl.edu
Address is the same as BAG

John C. Morris jcmorris@wustl.edu
Washington University School of Medicine
4488 Forest Park Avenue, Suite 130, Campus Box 8111
St Louis, Missouri 63108

Randall Bateman batemanr@wustl.edu
Washington University School of Medicine
660 South Euclid, Campus Box 8111
St. Louis, MO 63110

Tammie L.S. Benzinger benzingert@wustl.edu
Address is the same as TMB

Research in context

Evidence before this study
Using PubMed and Google Scholar the authors reviewed prior work on longitudinal neuroimaging markers of Alzheimer pathology with a focus on autosomal dominant Alzheimer disease (ADAD). We searched for all articles prior to October 31st, 2017 with no language restrictions for the keywords Alzheimer's, Alzheimer, longitudinal, positron emission tomography, PET, MRI, atrophy, FDG, hypometabolism, familial, and autosomal. Theories proposed initially in 2010 by Jack and colleagues and revised in 2013 posited temporal trajectories of Alzheimer biomarkers relative to each other and clinical decline. Work by Bateman and colleagues in 2012, Benzinger and colleagues in 2013, and Fleisher and colleagues in 2015 depict such temporal ordering of biomarkers in ADAD populations derived from cross-sectional analyses. There was also a small subset of longitudinal ADAD studies, but these had one or more limitation such as small populations (n<50), examination of only one biomarker, not accounting for regional differences or correlations in the brain, or had a short duration of longitudinal followup.

Added value of this study
Our study presents the first known work examining both the longitudinal temporal trajectories and spatial patterns of Alzheimer pathology in ADAD cohorts using neuroimaging. This work also presents the largest known cohort to date of ADAD individuals studied longitudinally with multiple neuroimaging biomarkers. Longitudinal analyses can provide a more accurate and powerful way to model the temporal emergence of pathology in ADAD. We find that mutation carriers first display Aβ accumulation, followed by hypometabolism, and finally structural atrophy; this is consistent with theoretical models and cross-sectional estimates from ADAD. Most importantly we consider such temporal relationships not in one singular summary measure, but characterize these trajectories throughout the brain. We found that the accrual of pathology varied throughout the brain and by modality in terms of the time of initial emergence and the rates of longitudinal change. These findings suggest region specific vulnerabilities to β-amyloidosis, metabolic decline, and atrophy that change over the course of the disease.

Implications of all the available evidence
Our results build upon existing evidence characterizing biomarkers in clinical and preclinical Alzheimer disease. Our findings suggest that imaging biomarkers follow a sequential pattern, with β-amyloidosis, hypometabolism, and structural atrophy emerging more than twenty, fifteen, and ten years respectively before the expected onset of dementia. Although there is a general hierarchical pattern, there was considerable regional heterogeneity. Most commonly, regions demonstrated an increase in β-amyloidosis and structural atrophy, but there was not evidence of metabolic declines. Further, rather than being homogenous, the same biomarker often demonstrates different longitudinal trajectories across brain regions. Characterizing the temporal and regional dynamics provides insight into disease pathophysiology. This information is critical to decide how to best use neuroimaging biomarkers in clinical trials for subject selection as well as outcomes measures.

Abstract

Background

Models of Alzheimer disease propose a sequence of amyloid-β (Aβ) accumulation, hypometabolism, and structural declines that precede the onset of clinical dementia. These pathological features evolve both temporally and spatially in the brain. This study aimed to characterize where in the brain and when in the course of the disease neuroimaging biomarkers become abnormal.

Methods

We analyzed data ~~collected~~ from mutation non-carriers, asymptomatic carriers, and symptomatic carriers collected between January 1st 2009 and December 31st 2015 from families carrying *PSEN1*, *PSEN2*, or *APP* mutations enrolled in the Dominantly Inherited Alzheimer's Network. We analyzed [11C]Pittsburgh Compound B positron emission tomography (PiB PET), [18F]Fluorodeoxyglucose (FDG PET), and structural magnetic resonance imaging (MRI) data using regions of interest to assess change throughout the brain. We estimated rates of biomarker change as a function of estimated years from symptom onset at baseline using linear mixed-effects models and determined the earliest point at which biomarker trajectories differed between mutation carriers and non-carriers.

Findings

PiB PET was available for 346 individuals, with 162 having longitudinal imaging; FDG PET was available for 352 (175 longitudinal); and MRI data was available for 377 (201 longitudinal). We found a sequence to pathological changes, with rates of Aβ deposition in mutation carriers being significantly different from non-carriers ~~occurring~~ first (on average across significant regions at -18·9 (sd 3·3) years before expected onset), followed by hypometabolism (-14·1 years, sd 5·1) and lastly structural declines (-4·7 years, sd 4·2). This biomarker ordering was preserved in most, but not all, regions. The temporal emergence within a biomarker varied across the brain, with the precuneus being the first cortical region in each modality to show divergence between groups. ~~, although the ordering across biomarkers was preserved in most, but not all, regions.~~

Interpretation

Mutation carriers had elevations in Aβ deposition, reduced glucose metabolism, and cortical thinning which preceded the expected onset of dementia. We found that the accrual of these pathologies varied throughout the brain, suggesting differential regional and temporal vulnerabilities to Aβ, metabolic decline, and structural atrophy. This provides insight into the temporal and spatial development of pathological change in Alzheimer disease. Understanding where and when pathology accrues in the brain is key for using biomarkers in a clinical setting as well as designing and evaluating clinical trials.

Funding

National Institutes of Health UFAG032438, UL1TR000448, P30NS098577, R01EB009352, and NS080675, the German Center for Neurodegenerative Diseases, and the Medical Research Council Dementias Platform UK (MR/L023784/1 and MR/009076/1). ClinicalTrials.gov number, NCT00869817

Formatted: Superscript

Formatted: Superscript

Introduction
Alzheimer disease (AD) presents as a progressive loss of cognitive function, leading to severe impairment and loss of independence. AD's long preclinical phase has bolstered efforts to identify *in vivo* biomarkers to aid disease diagnosis and prognosis[1]. Models of AD pathophysiology theorize a temporal sequence where disruptions in amyloid-β (Aβ) production and/or clearance initiate a biological cascade that leads to Aβ plaque formation that spreads throughout the cortex followed by tauopathy, neuronal dysfunction and death, and ultimately dementia[2,3].

Positron emission tomography (PET) and magnetic resonance imaging (MRI) can assess both the amount and location of Aβ plaques, tauopathy (neurofibrillary tangles, neuritic plaques, and neuropil), altered glucose metabolism, and structural decline. The temporal sequence of these biomarkers provides information about the pathogenesis of AD. Determining the ordering of changes in sporadic AD is problematic, as it is difficult to predict an individual's relative position in the disease. Autosomal dominant AD (ADAD) is well suited to study biomarker trajectories due to the virtually complete penetrance of the mutations and consistency of symptom onset within families[4,5]. The conserved onset age within families and mutation types allows individuals to be staged relative to their expected onset of symptoms.

~~Cross-sectional~~ ADAD work ~~on ADAD~~ has revealed a temporal ordering of biomarkers ~~that is~~ consistent with theoretical models,[6–8] and indications that pathology progressively appears in new regions of the brain as the disease worsens[7]. This has primarily relied on cross-sectional analyses, with limited analyses of modest longitudinal cohorts[7,9–16]. Longitudinal analyses can provide a better estimate of the true pathological trajectories~~Longitudinal analyses can better estimate temporal dynamics and typically have more power to detect significant differences than cross-sectional analyses.~~[17,18] ~~, as within-subject measures reduce between-subject variability caused by unmodeled individual differences. Longitudinal analyses can provide a better estimate of the true pathological trajectories occurring in the disease.~~ This is critical~~ly important~~ as interventional ~~clinical~~ trials ~~in~~ such as the Dominantly Inherited Alzheimer Network

(DIAN) trials unit,[19] the Alzheimer's Prevention Initiative (API),[20] and the Anti-Amyloid Treatment in Asymptomatic Alzheimer's Study (A4)[21] will all evaluate alterations in longitudinal biomarker trajectories ~~over time~~. ~~Further, it is critical to understand how such temporal trajectories varies across the brain, as some regions may be more suitable for studying the efficacy of treatment than others.~~

The DIAN observational study (DIAN)[4] has established a large cohort of ADAD ~~individuals from~~ families ~~with ADAD who obtain~~with longitudinal Aβ, metabolic, and structural neuroimaging assessments. Our current work compares rates of biomarker change in a large population of mutation carriers (MC) and non-carriers (NC) throughout the entire brain. ~~Although these modalities are often represented with aggregate summary measures, there are distinct spatial appearances and regional evolutions of each pathology[7,22,23]. Studying spatial patterns of longitudinal change provides information about local vulnerabilities to pathology that are lost when using summary measures.~~

~~Our current work compares rates of biomarker change in a large population of mutation carriers (MC) and non-carriers (NC). Using linear mixed effects models, we compare biomarker change not using one summary measure, but throughout the brain.~~ In this way we can visualize when pathology biomarkers first emerge and how they spread throughout the course of the disease. ~~Clarifying changes in spatial patterns of biomarker accumulation over time will advance our understanding of disease pathobiology and provide critical information for the design and interpretation of disease-modifying clinical trials using biomarkers to enrich enrollment or as endpoints.~~

Methods

Participants

Individuals from families known to have mutations in the presenilin 1 (*PSEN1*), presenilin 2 (*PSEN2*), and amyloid precursor protein (*APP*) genes were recruited from 14 performance sites participating in the DIAN observational study (http://www.dian-info.org). Participants were recruited from DIAN sites in the United States, Great Britain, Germany, and Australia between January 1st 2009 and December 31st 2015. All

participants with genetic, clinical, and neuroimaging data that passed quality control from the tenth semiannual data freeze were included in the analyses. The institutional review board at Washington University in St. Louis provided supervisory review and human studies approval. Participants or their caregivers provided written informed consent in accordance with their local institutional review board. Clinical and imaging visits in DIAN ~~were~~ are performed every three years for asymptomatic individuals until they are within three years of their parental age of dementia onset. Assessments become annual once an individual is within three years of parental age at onset or if an individual becomes symptomatic. Analyses excluded families with the Dutch and Flemish Mutation, as these APP mutations often present with predominant cerebral amyloid angiopathy and diffuse Aβ plaques (see supplemental material). The analyses included 346 individuals with Aβ PET data, 352 with PET metabolism data, and 377 with MRI~~;~~. ~~See Table 1 for baseline demographics.~~

Clinical Assessment.

Dementia status was assessed using the Clinical Dementia Rating (CDR)[22]. For each visit a participant's estimated years from expected symptom onset (EYO) was calculated based upon the participant's current age relative to either the family mutation specific expected age at dementia onset[5]~~,~~ or parental age at first progressive cognitive decline if mutation age at onset was unknown. A "mutation specific" expected age of dementia onset is calculated by averaging the age of onset reported in the literature across individuals with the same specific mutation[5]. EYO is established identically for both carriers and non-carriers. The presence or absence of an ADAD mutation was determined using PCR-based amplification of the appropriate exon followed by Sanger sequencing[6]. Clinical evaluators were blind to participant mutation status.

MRI.

MRI was performed using the Alzheimer's Disease Neuroimaging Initiative (ADNI) protocol[23]. Sites used a 3T scanner and were required to pass regular quality control assessments. T1-weighted images (1·1 x 1·1 x 1·2-mm voxels) were acquired for all subjects. The ADNI Imaging Core screened images for protocol compliance and artifacts.

Volumetric segmentation and cortical surface reconstruction was performed using FreeSurfer 5·3[24,25] which automatically defines subcortical and cortical regions of interest (ROIs). Segmentations were inspected by members of the DIAN Imaging Core and edited as needed. Subcortical volumes were corrected for intracranial volume using a regression approach. Cortical thickness and volume measures were averaged across hemispheres. The cortical and subcortical labels identified on the MRI were utilized for the regional processing of all PET data. For all analyses we examined 34 cortical ROIs and 7 subcortical ROIs. A full list of regions is available in supplemental material.

PET.

Aβ imaging was performed using a bolus injection of [^{11}C]Pittsburgh Compound B (PiB). Acquisition consisted of a 70-minute scan starting at injection or a 30-minute scan beginning 40 minutes post-injection. Data in the common 40–70 minute time frame was converted to regional standardized uptake value ratios (SUVRs) relative to the cerebellar grey matter using FreeSurfer derived regions of interest[26] (PET Unified Pipeline, https://github.com/ysu001/PUP). Metabolic imaging was performed with [^{18}F]Fluorodeoxyglucose (FDG) with a 30-minute dynamic acquisition beginning 30 minutes after injection. Data from the last 20 minutes of each FDG scan were converted to SUVRs relative to cerebellar grey. Both types of PET data were partial volume corrected using a regional spread function technique[27,28].

As there were no *a priori* laterality predictions, data were averaged across hemispheres before being entered into statistical analyses. Differences in spatial resolution across PET scanners were accounted for by applying scanner specific spatial filters to achieve a common resolution (8 mm)[29]. The ADNI PET Core verified that PET images were acquired using the established protocol and substantially free of artifacts.

Statistical Analyses

We used multivariate linear mixed effects (LME) models ~~in order~~ to describe the evolution of Alzheimer disease biomarkers. LME models have many benefits ~~in longitudinal settings,~~ including providing a flexible approach to deal with an unequal

4

number of measurement points or intervals. While neuroimaging analyses traditionally use univariate models, the field has begun using multivariate models which account for correlations between regional or voxelwise measurements[30–32]. Multivariate LME models can increased statistical power and reliability compared to univariate methods[30,31]. We implemented a Bayesian multivariate LME model to directly compare longitudinal biomarker changes across brain regions. Cortical and subcortical measurements were analyzed separately for each modality (PiB, FDG, and volumetric), resulting in total of six independent models.

The full Bayesian LME model is described in ~~detail in~~ the supplemental material. Each region included fixed effects for mutation status, time from baseline, baseline EYO, and all possible two and three-way interactions. EYO was modeled as a restricted cubic spline with knots at the 0·10, 0·50, and 0·90 quantiles. We chose restricted cubic splines to model EYO as they represent a flexible approach for accounting for nonlinearities in the data without forcing any particular curve shape. Splines have also been used extensively in the literature to model longitudinal changes in Alzheimer disease biomarkers[33,34]. For every region we included random intercepts and slopes at the subject-level, as well as random intercepts for family affiliation. At the subject-level, covariance matrices were constructed so that intercepts and the slopes were allowed to correlate across all regions in a model.

To fit each model we used Stan (http://mc-stan.org/)[35,36], an open source package for Hamilton Markov chain Monte Carlo analyses. A parameter, or combination of parameters, was considered statistically significant if the 99% equal-tailed credible intervals of the posterior distribution did not overlap zero. Analyses were run separately for each modality (MRI, PiB, and FDG). Within each modality one model simultaneously fit 34 cortical ROIs and a second model simultaneously fit 7 subcortical ROIs derived from FreeSurfer. Each regional comparison within a model is simply a different slice of the same multidimensional posterior distribution. The current analyses focus on the interaction between mutation status and the longitudinal rate of change. Including multiple regions within one model also allows for the direct comparison of rates of

5

changes between regions (supplemental material).

Role of the funding source

The study sponsors had no role in the study design, data collection, data analysis, data interpretation, writing of the report, or the decision to submit the manuscript for publication. All coauthors had full access to the data in the study and the corresponding author had final responsibility for the decision to submit for publication.

~~An example of one region is shown in Figure 1. For the both the middle and right-hand panels the shaded areas represent 99% credible intervals around the model estimates. The credible intervals are drawn from the actual distributions of model fits derived by the Hamilton Markov Chain Monte Carlos analyses. Any point in the difference curves (right-hand panels) where the shaded area is not touching the zero axis is a point in the disease progression (as measured by EYO) where the biomarker rate of change is different between groups. The first EYO point that was significantly different between groups was considered the initial diverge between groups. Figures depicting the model results for every ROI are available in supplemental materials. To avoid inadvertently revealing mutation status figures are displayed with baseline EYO -29 to +10.~~

Results

Population demographics are in Table 1. Subjects with longitudinal data had an average of 2·4 visits (sd 0·8) and 2·7 (sd 1·1) years of data. Figure 1 shows example LME model fits for one region. ~~An example of one region is shown in Figure 1.~~ For the both the middle and right-hand panels the shaded areas represent 99% credible intervals around the model estimates. The credible intervals are drawn from the actual distributions of model fits derived by the Hamilton Markov Chain Monte Carlos analyses. Any point in the difference curves (right-hand panels) where the shaded area is not touching the zero axis is a point in the disease progression (as measured by EYO) where the biomarker rate of change is different between groups. The first EYO point that was significantly different between groups was considered the initial diverge between groups. Figures depicting the model results for every ROI are available in supplemental materials. To

avoid inadvertently revealing ~~mutation~~participants' mutation status ~~figures~~at the edges of our sample where there are only a few individuals, figures are displayed with baseline EYO -29 to +10.

~~As an example of one region Figure 1 shows the model fits for the precuneus stratified by mutation status.~~ The rate of Aβ accumulation is statistically higher in MC relative to NC participants starting more than two decades (EYO -22·2) before the expected age of dementia onset (Figure 1). As glucose utilization represents a natural biological property it contains both maturational and disease-related trajectories. In both groups, the precuneus FDG trajectories were initially positive, became neutral, and then negative. This negative directional acceleration begins earlier and was larger in MCs, with the rate of change becoming significantly less than NC at EYO -18·8. Finally, precuneus cortical thinning significantly differs in MC relative to NC at EYO -13·0. Supplemental material contains results for every ROI. Overall, in regions with a significant effect relative to NC, rates of Aβ deposition were significantly higher in MC at an average EYO of -18·9 (sd 3·3), metabolism began declining at an average EYO of -14·1 (sd 5·1), and MRI structural measures declined at an average EYO -4·7 (sd 4·2).

Figure 2 depicts EYOs when and whether the longitudinal rate of change first differs between MC and NC for each biomarker. The differences across regions and modalities reflect the temporal and spatial evolution of pathology over the course of the disease. Rates of biomarkers change in regions that are grey are never significantly different between groups. This information is presented in numeric form in Supplemental Tables 1 and 2. While many regions follow trajectories similar to the precuneus, the emergence of pathology varied throughout the brain. Further, there were regional differences by modality, for example, relative to NC the superior temporal lobe did not demonstrate a metabolic loss, but had atrophy changes at -5·6 EYO. Figure 3 depicts rates of change in MC for three cortical and three subcortical regions that exemplify common patterns ~~seen across regions~~.

For PiB PET, 32/34 cortical regions showed significantly greater longitudinal rates of accumulation in MC relative to NC. The first point of divergence between groups varied across regions (EYO -22·2 to -2·5), with the precuneus, posterior cingulate gyrus, and medial orbital frontal cortex regions showing the earliest changes (~EYO -21). Of the 32 regions with significant differences, all but the cuneus (-2·5) occurred prior to an EYO of -15. In the seven subcortical regions the accumbens (-22·2), putamen (-17·0), and caudate (-16·4) demonstrated greater PiB accumulation rates in MC while the amygdala, hippocampus, palladium, and thalamus did not differ. Significant differences in progressive hypometabolism in MC relative to NC were less pronounced, with 8/34 cortical regions demonstrating significant interactions. The effects ranged from EYO -18·8 to -2·8, with the earliest effects detected in the precuneus, banks of the superior temporal sulcus, and caudal middle frontal cortex (EYO ~-18). No subcortical regions showed significant differences in the rate of FDG change. For MRI 24/34 cortical and 4/7 subcortical areas demonstrated increased rates of atrophy in MC relative to NC with effects appearing from EYO -13·0 to 2·3. The precuneus (-13·0), banks of the superior temporal sulcus (-11·5), and inferior parietal cortex (-10·6) demonstrated the earliest changes.

We also observed regional differences in the rates of biomarker change within the MC group. In the precuneus there was a rapid increase in Aβ deposition; this rate peaked but remained positive even after the predicted onset of dementia (Figure 3 and Figure 4). This was the most common pattern across areas. In other regions (e.g. insula) initial accelerations in Aβ deposition were followed by decelerations, leading to a plateau of total Aβ levels. In a subset of regions (e.g. inferior temporal cortex) the estimated rate of Aβ accumulation accelerates throughout the disease. Once ~~it began to decline~~declining, glucose metabolism in the precuneus showed prominent, worsening rates of hypometabolism before the rates~~a constant rate of decline~~stabilized (~ EYO -5), while in inferior temporal cortex the rate of metabolic loss modestly increased initially before quickly plateauing ~~later on in the disease~~ (Figure 3B). Many regions had relatively small rates of metabolic decline in MC, even at later EYOs. In regions with structural decline the trajectories were fairly consistent, with the rate of atrophy accelerating as the disease

8

progressed. However, the absolute rate of decline was often different between regions. Matrices directly comparing the regional rates of change for each biomarker at different EYOs (-25, -15, -5, and 5) can be found in supplemental material. Voxel-wise movies depicting the rate of change and total biomarker levels in MC at every EYO and the creation of these movies are is detailed in supplemental material.

Discussion

AD is not a static disease but possesses dynamism in terms of what pathological processes first appear, and how such pathology propagates throughout the brain. As dementia onset is predictable in ADAD, it provides an elegant model with which to examine pathological staging. Characterizing the spatial and temporal spread of pathology provides insight to the pathophysiology of the disease, informs how neuroimaging could aid optimal subject recruitment in clinical trials, and is critical to measure the efficacy of interventions on longitudinal biomarker measurements.

The primary goal of the current analysis was to find the first biomarker time point in the course of the disease where carriers of ADAD mutations demonstrated different rates of pathological progression relative to non-carrier family members. This time point can be interpreted as the moment where the longitudinal change in that brain area due to AD can first be detected with *in vivo* neuroimaging. The primary questions using this approach focused on regional differences across the brain within a marker (e.g. precuneus vs. parietal Aβ PET) as well as comparing spatial differences between biomarkers (e.g. Aβ PET vs. FDG PET).

Consistent with prior work in the field we found that Aβ deposition was the first biomarker to demonstrate differences between mutation groups. MC had greater Aβ deposition more than 20 years before the expected age of symptom onset. Aβ increases were near ubiquitous, with most regions changing more than 14 years before the expected year of dementia. Measures of metabolism in ADAD represent overlapping maturational and disease changes. Both NC and MC cohorts had inverted U-shaped trajectories (Figure 1D & 1E), with the absolute levels of glucose metabolism initially modestly

9

increasing with EYO, followed by a prolonged decrease. The key difference is that MC showed metabolic reductions earlier and to a greater degree than NC. While cross-sectional values still overlapped between groups early in the disease, longitudinal trajectories reveal divergence (supplementary material). The precuneus demonstrates the earliest metabolic decrease ~~in the brain at~~ an EYO of -18·8, with significant regions on average becoming abnormal at EYO -14·1. Reductions in grey matter ~~integrity~~ were the last neuroimaging biomarker to manifest and occured over the majority of the brain. Again the precuneus is one of the earliest regions to change, with declines emerging a decade before estimated dementia onset, while overall declines were most prolific in the five years preceding ~~the~~ expected dementia onset. The direct comparison of the rates of biomarker change between regions is presented in supplementary material.

The relationships between the three biomarkers are complex. While all regions ~~that showed~~with metabolic decreases have abnormal ~~rates of~~ Aβ accumulation, many regions with abnormal Aβ accumulation rates did not demonstrate elevated metabolic decline. Although FDG hypometabolism and structural decline are markers of degeneration, our results indicate they can be incongruent. In regions where they both occur, declines in glucose metabolism ~~can~~ precede atrophy by ~5 to 10 years. However, there are regions that demonstrated β-amyloidosis and structural atrophy where significant metabolic decline was not detected (e.g. occipital and temporal regions). Portions of the medial temporal lobe (e.g. the hippocampus) did not manifest pathological change in Aβ or FDG, but had structural declines. Although there is generally a tripartite hierarchy such that β-amyloidosis precedes metabolic decline that in turn precede atrophy, these relationships are highly heterogeneous across the cortex.

Discordance between imaging biomarkers has been noted in ~~studies of~~ sporadic AD [37–44]. Due to the cross-sectional nature of the majority of the work ~~in the field~~, such spatial incongruences could be due to temporal lags in the emergence of pathologies. ~~Work looking at cross-model relationships between baseline and longitudinal follow-up has shown such phenomena.~~ [42,44] EYO, as a marker of disease time, is perfectly suited to detect such temporal evolutions. The current work does indeed clearly demonstrate that a

temporal progression is present in some regions (e.g. PiB, FDG, and cortical thinning in the precuneus). However, despite the long disease window covered by the current study population, some region still only demonstrate a subset of pathologies. This suggests the incongruences are not simply a product of temporal lag, but can represent true ~~pathological~~ heterogeneity. Other, unobserved, biomarkers such as those that measure tau pathology and inflammation, may help explain this heterogeneous relationship.

The current work presents the largest and most comprehensive analysis of neuroimaging data in ADAD to date. Still, the majority of longitudinal subjects had only a limited follow-up (average 2·4 visits); results at the edges of the EYO range where outliers have disproportional influence must be interpreted with care. ~~and t~~There are also only modest numbers of subjects with PSEN2 and APP mutations.~~-~~ As the DIAN study gains more time points longitudinal estimates will be improved further and it may ~~also~~ be possible to ~~examine patterns of change between~~compare the three types of mutations. A greater number of individuals and time points will also increase the feasibility of modeling multiple modalities simultaneously across all brain regions as previously done using summary measures of pathology.[45]

The temporal and spatial ordering of biomarkers must also be interpreted with caveats. No one individual has data across the entire disease window, and our results represent population rather than individual subject effects. Further, as seen in regional fits (Figure 1 and supplemental material) some individuals differ from population trajectories. Thus, imaging data alone may not be sufficient to make individual-level disease stage predictions. Such predictions would require further work that accounts for individual differences due to factors such as genetic variability and lifestyle. The current work also utilizes partial volume corrected PET data,[27,28] analyses without this step could have slightly different trajectories late in the disease.

The temporal ordering of biomarker change must also be viewed as relative rather than absolute. Our models are fit using a particular definition of EYO. Supplemental models using a ~~slightly~~ modified definition of EYO indicate a preserved relative ordering (e.g.

precuneus Aβ > hypometabolism > structural decline) but slight differences in absolute timing (e.g. ~~precuneus PiB divergence~~ shifts from EYO -22·2 to -19·8). Further, our results reflect the first *detectable* changes with PET and MRI, which are constrained by the inherent sensitivities and signal to noise properties of the imaging techniques. The current analyses utilize the cerebellum as a reference region for PET. Results using the brainstem instead were essentially unchanged (Supplementary Tables 3 and 4). Finally, although ADAD can serve as a model for sporadic AD, direct comparisons must explore potential differences.

Our results reveal complex patterns of biomarker accumulation across the brain. Elevations in β-amyloidosis occur more than two decades before and continue to accrue even after the expected year of symptom onset. Neurodegeneration measured with both FDG and structural MRI begins while Aβ is still increasing and occurs closer in time, but still well before the onset of dementia. While global measures likely capture a large degree of intraindividual variability, our results indicate not just when, but where pathology emerges in the brain. Understanding such longitudinal change provides insight into the pathophysiological progression of AD and has ~~important~~ implications for clinical trials ~~utilizing neuroimaging~~.

Contributors

BAG and TMB equally contributed to the present work and wrote the manuscript, analyzed the data, and generated the figures and movies. YS, AH, AD, SF, JC, CRJ, and MMW oversaw data quality control and processing. CX, NJC, JH, DSM, AMF, DMH, RCH, KLP, EM, GW, MER, JCM, RJB, and TLSB and oversaw overall study design and general implementation. RJB and TLSB assisted in data interpretation. BMA, SBB, AMB, DMC, JPC, SC, StF, NCF, NRG, CF, JL, CLM, MNR, SS, AJS, PRS, and PMT oversaw study implementation and data collection at their respective institutions. All authors revised the manuscript.

Declarations of Interest

BAG and BMA report participating in a clinical trial of AV-1451 sponsored by Avid

Acknowledgements

15

Figure 1: Modeling longitudinal change in the precuneus for PiB (top), FDG (middle), and cortical thickness (bottom). The left-hand panels (A, D, & G) depict the model estimates of longitudinal biomarkers. The middle panels (B, E, & H) depict the estimated rate of change across the course of the disease for mutation carriers and non-carriers. Individual random effect slope estimates are plotted as colored dots. The right hand panels (C, F, and I) depict the difference in rate of biomarker change between mutation carriers and non-carriers across the course of the disease. For both the middle and right-hand panels the shaded areas represent 99% credible intervals around the model estimates. Any point in this difference curves where the shaded area is not touching the zero axis is a point in the disease progression (as measured by EYO) where the biomarker accumulation rate is different between groups. Figures depicting the model results for every ROI are available in supplemental materials. To avoid inadvertently revealing mutation status figures are displayed with baseline EYO -29 to +10.

Figure 2: Emergence of neuroimaging biomarkers. The color scale represents the first point in the disease relative to estimated age at onset (EYO) where rates of biomarker change in that cortical region are significantly different between mutation carriers and non-carriers (akin to the first point where credible interval are different from zero in Figure 1 right panels). There is a temporal evolution where increased Aβ deposition precedes hypometabolism that in turn is followed by cortical thinning. Information for all modalities and regions is presented in numeric form in Supplemental Tables 1 and 2.

Figure 3: Trajectories of biomarker accumulation in mutation carriers for three cortical (top) and three subcortical regions (bottom) for PiB (left), FDG (middle), and structural MRI (right) that highlight different patterns of change seen in different brain regions.

Figure 4: Depictions of model estimates of rate of change in PiB (top), FDG (middle), and cortical thickness (bottom) in mutation carriers at an EYO of -25, -15, -5, and +5.

~~**Movie 1:** Voxel-wise change for beta-amyloid deposition by PiB PET in mutation carriers. The top panel of the figure shows the rate of change at each EYO. The bottom panel depicts the total biomarker levels at each EYO for mutation carriers derived by~~

integrating the rate of change and adding it to the baseline value of a mutation carrier at an EYO of -25 and time zero.

Movie 2: Voxel-wise change in FDG PET uptake in mutation carriers. The top panel of the figure shows the rate of change at each EYO. The bottom panel depicts the total biomarker levels at each EYO for mutation carriers derived by integrating the rate of change and adding it to the baseline value of a mutation carrier at an EYO of -25 and time zero.

Movie 3: Voxel-wise change in cortical thickness by MRI in mutation carriers. The top panel of the figure shows the rate of change at each EYO. The bottom panel depicts the total biomarker levels at each EYO for mutation carriers derived by integrating the rate of change and adding it to the baseline value of a mutation carrier at an EYO of -25 and time zero.

Table 1: Study demographics at baseline.

Demographics at Baseline			
	Non-Carriers	Asymptomatic Carriers	Symptomatic Carriers
Number	148	141	88
Females (%)	85 (57%)	78 (55%)	49 (56%)
Age (years/sd)	39·5 (11·4)	34·6 (9·2)	45·7 (9·9)
MMSE (mean/sd)	29·0 (2·7)	28·8 (2·7)	23·9 (10·2)
CDR-SOB (mean/SD)	0·0 (0·2)	0·0 (0·1)	3·6 (3·5)
EYO (years/sd)	-8·9 (11·4)	-13·7 (9·2)	0·5 (7·1)
PSEN1/PSEN2/APP	122/17/9 (82/11/6%)	117/16/8 (83/11/6%)	76/6/6 (86/7/7%)
N with Follow up (%)	70 (47%)	73 (52%)	58 (66%)
N of visits*(sd)	2·3 (0·8)	2·3 (0·8)	2·8 (1·2)
~~Duration~~ Follow up in years* (sd)	3·0 (1·7)	3·0 (1·6)	2·0 (1·3)

Summary of Imaging Data			
Data By Modality	PIB	FDG	MRI
1 visit	184	177	176
2 visits	124	131	145
3 visits	23	27	35
4 visits	10	11	11
5 visits	4	5	8
6 visits	1	1	2
Total Subjects	346	352	377

*Summary values are only for those individuals with longitudinal data
EYO - estimated years to dementia onset
MMSE –Mini Mental State Examination
CDR-SOB – Clinical Dementia Rating Sum of Boxes

References

1 Pike KE, Savage G, Villemagne VL, *et al.* β-amyloid imaging and memory in non-demented individuals: evidence for preclinical Alzheimer's disease. *Brain* 2007; **130**.

2 Hardy JA, Higgins GA. Alzheimer's disease: The amyloid cascade hypothesis. Science (80-.). 1992; **256**: 184–5.

3 Jack CR, Knopman DS, Jagust WJ, *et al.* Tracking pathophysiological processes in Alzheimer's disease: an updated hypothetical model of dynamic biomarkers. *Lancet Neurol* 2013; **12**: 207–16.

4 Moulder KL, Snider BJ, Mills SL, *et al.* Dominantly Inherited Alzheimer Network: facilitating research and clinical trials. *Alzheimers Res Ther* 2013; **5**: 48.

5 Ryman DC, Acosta-Baena N, Aisen PS, *et al.* Symptom onset in autosomal dominant Alzheimer disease: a systematic review and meta-analysis. *Neurology* 2014; **83**: 253–60.

6 Bateman RJ, Xiong C, Benzinger TLS, *et al.* Clinical and biomarker changes in dominantly inherited Alzheimer's disease. *N Engl J Med* 2012; **367**: 795–804.

7 Benzinger TLS, Blazey T, Jack CR, *et al.* Regional variability of imaging biomarkers in autosomal dominant Alzheimer's disease. *Proc Natl Acad Sci U S A* 2013; **110**: E4502-4509.

8 Fleisher AS, Chen K, Quiroz YT, *et al.* Associations between biomarkers and age in the presenilin 1 E280A autosomal dominant Alzheimer disease kindred: a cross-sectional study. *JAMA Neurol* 2015; **72**: 316–24.

9 Yau W-YW, Tudorascu DL, McDade EM, *et al.* Longitudinal assessment of neuroimaging and clinical markers in autosomal dominant Alzheimer's disease: a prospective cohort study. *Lancet Neurol* 2015; **14**: 804–13.

10 Weston PSJ, Nicholas JM, Lehmann M, *et al.* Presymptomatic cortical thinning in familial Alzheimer disease: A longitudinal MRI study. *Neurology* 2016; : 10.1212/WNL.0000000000003322.

11 Wang F, Gordon BA, Ryman DC, *et al.* Cerebral amyloidosis associated with cognitive decline in autosomal dominant Alzheimer disease. *Neurology* 2015; published online Aug 5. DOI:10.1212/WNL.0000000000001903.

12 Sala-Llonch R, Llad? A, Fortea J, *et al.* Evolving brain structural changes in PSEN1 mutation carriers. *Neurobiol Aging* 2015; **36**: 1261–70.

13 Schott JM, Fox NC, Frost C, *et al.* Assessing the onset of structural change in familial Alzheimer's disease. *Ann Neurol* 2003; **53**: 181–8.

14 Fagan AM, Xiong C, Jasielec MS, *et al.* Longitudinal change in CSF biomarkers in autosomal-dominant Alzheimer's disease. *Sci Transl Med* 2014; **6**: 226ra30.

15 Knight WD, Kim LG, Douiri A, Frost C, Rossor MN, Fox NC. Acceleration of cortical thinning in familial Alzheimer's disease. *Neurobiol Aging* 2011; **32**: 1765–73.

16 Kinnunen KM, Cash DM, Poole T, *et al.* Presymptomatic atrophy in autosomal dominant Alzheimer's disease: a serial MRI study. *Alzheimer's Dement*.

17 Thompson WK, Hallmayer J, O'Hara R, Initiative the ADN. Design Considerations for Characterizing Psychiatric Trajectories Across the Lifespan: Application to Effects of APOE-ε4 on Cerebral Cortical Thickness in Alzheimer's

Disease. *Am J Psychiatry* 2011; **168**: 894–903.

18   Xu Z, Shen X, Pan W, *et al.* Longitudinal analysis is more powerful than cross-sectional analysis in detecting genetic association with neuroimaging phenotypes. *PLoS One* 2014; **9**: e102312.

19   Mills SM, Mallmann J, Santacruz AM, *et al.* Preclinical trials in autosomal dominant AD: implementation of the DIAN-TU trial. *Rev Neurol (Paris)* 2013; **169**: 737–43.

20   Reiman EM, Langbaum JBS, Fleisher AS, *et al.* Alzheimer's Prevention Initiative: a plan to accelerate the evaluation of presymptomatic treatments. *J Alzheimers Dis* 2011; **26 Suppl 3**: 321–9.

21   Sperling R a A, Rentz DMM, Johnson K a A, *et al.* The A4 Study: Stopping AD before Symptoms Begin? *Sci Transl Med Med* 2014; **6**: 228fs13-228fs13.

22   Morris JC. The Clinical Dementia Rating (CDR): Current version and scoring rules. *Neurology* 1993; **43**: 2412–4.

23   Jack CCR, Bernstein MA, Borowski BBJ, *et al.* Update on the magnetic resonance imaging core of the Alzheimer's disease neuroimaging initiative. *Alzheimer's Dement* 2010; **6**: 212–20.

24   Fischl B. FreeSurfer. *Neuroimage* 2012; **62**: 774–81.

25   Fischl B, Dale AMM. Measuring the thickness of the human cerebral cortex from magnetic resonance images. *Proc Natl Acad Sci U S A* 2000; **97**: 11050–5.

26   Su Y, D'Angelo GM, Vlassenko AG, *et al.* Quantitative Analysis of PiB-PET with FreeSurfer ROIs. *PLoS One* 2013; **8**: e73377.

27   Su Y, Blazey TM, Snyder AZ, *et al.* Partial volume correction in quantitative amyloid imaging. *Neuroimage* 2015; **107**: 55–64.

28   Rousset OG, Ma Y, Evans AC. Correction for partial volume effects in PET: Principle and validation. *J Nucl Med* 1998; **39**: 904–11.

29   Joshi A, Koeppe RA, Fessler JA. Reducing between scanner differences in multi-center PET studies. *Neuroimage* 2009; **46**: 154–9.

30   Bernal-Rusiel JL, Reuter M, Greve DN, Fischl B, Sabuncu MR. Spatiotemporal linear mixed effects modeling for the mass-univariate analysis of longitudinal neuroimage data. *Neuroimage* 2013; **81**: 358–70.

31   Bernal-Rusiel JL, Greve DN, Reuter M, Fischl B, Sabuncu MR. Statistical analysis of longitudinal neuroimage data with Linear Mixed Effects models. *Neuroimage* 2013; **66**: 249–60.

32   Bilgel M, Prince JL, Wong DF, Resnick SM, Jedynak BM. A multivariate nonlinear mixed effects model for longitudinal image analysis: Application to amyloid imaging. *Neuroimage* 2016; **134**: 658–70.

33   Jack CR, Wiste HJ, Lesnick TG, *et al.* Brain β-amyloid load approaches a plateau. *Neurology* 2013; **80**: 890–6.

34   Jack CR, Vemuri P, Wiste HJ, *et al.* Shapes of the trajectories of 5 major biomarkers of Alzheimer disease. *Arch Neurol* 2012; **69**: 856–67.

35   Carpenter B, Lee D, Brubaker MA, *et al.* Stan: A Probabilistic Programming Language. *J Stat Softw* 2016.

36   Gelman A, Lee D, Guo J. Stan: A Probabilistic Programming Language for Bayesian Inference and Optimization. *J Educ Behav Stat* 2015; **40**: 530–43.

37   Gordon BA, Blazey T, Benzinger TL. Regional variability in Alzheimer's disease

biomarkers. *Future Neurol* 2014; **9**: 131–4.

38   La Joie R, Perrotin A, Barré L, *et al.* Region-specific hierarchy between atrophy, hypometabolism, and β-amyloid (Aβ) load in Alzheimer's disease dementia. *J Neurosci* 2012; **32**: 16265–73.

39   Grothe MJ, Teipel SJ. Spatial patterns of atrophy, hypometabolism, and amyloid deposition in Alzheimer's disease correspond to dissociable functional brain networks. *Hum Brain Mapp* 2016; **37**: 35–53.

40   Edison P, Archer HA, Hinz R, *et al.* Amyloid, hypometabolism, and cognition in Alzheimer disease: an [11C]PIB and [18F]FDG PET study. *Neurology* 2007; **68**: 501–8.

41   Lehmann M, Ghosh PM, Madison C, *et al.* Diverging patterns of amyloid deposition and hypometabolism in clinical variants of probable Alzheimer's disease. *Brain* 2013; **136**: 844–58.

42   Förster S, Grimmer T, Miederer I, *et al.* Regional Expansion of Hypometabolism in Alzheimer's Disease Follows Amyloid Deposition with Temporal Delay. *Biol Psychiatry* 2012; **71**: 792–7.

43   Alexopoulos P, Kriett L, Haller B, *et al.* Limited agreement between biomarkers of neuronal injury at different stages of Alzheimer's disease. *Alzheimer's Dement* 2014; **10**: 684–9.

44   Förster S, Yousefi BH, Wester H-J, *et al.* Quantitative longitudinal interrelationships between brain metabolism and amyloid deposition during a 2-year follow-up in patients with early Alzheimer's disease. *Eur J Nucl Med Mol Imaging* 2012; **39**: 1927–36.

45   Donohue MC, Jacqmin-Gadda H, Le Goff M, *et al.* Estimating long-term multivariate progression from short-term data. *Alzheimer's Dement* 2014; **10**: S400–10.

Supplemental Text

Statistical Methods

Longitudinal neuroimaging data is often modeled using repeated measures analysis of variance or cross-sectional analyses of a summary measurement representing longitudinal trajectories such as annualized percent change. Such approaches do not appropriately account for the covariance structure introduced by serial measurements and cannot adequately cope with imperfect timing or unbalanced number of data points[1] as is present in the current dataset. Linear mixed-effects (LME) models are a powerful and versatile approach to longitudinal analyses of neuroimaging data[2]. The central idea in LME models is to allow a subset of regression parameters to vary randomly across subjects. The longitudinal trajectory is modeled as a combination of population-level "fixed" effects and subject-specific "random" effects allowing for the analysis of between-subject and within-subject sources of variability, which allows subjects to have an unequal number of visits or variable intervals between observations. Such models also allow individuals with only one time point to contribute to the estimation of all parameters that do not contain longitudinal components (e.g. the main effect of baseline EYO). This maximizes the statistical power by utilizing the entire available sample. Extensions of the LME framework to neuroimaging data include models that account for the spatiotemporal dependencies among neighboring locations[3].

The general form of our Bayesian multivariate LME model is given by:

$$Y_{ijk} \sim Normal(X_{ijk}\beta + \gamma_{ik} + Z_{ijk}\delta_{ik} + \theta_k, \Sigma) \ (1)$$

where Y_{ijk} is a row vector of R regional responses for subject i at time point j within family k. X_{ijk} is a row vector of P fixed effects regressors and β is a P by R matrix of fixed effects coefficients. Prior to model fitting all data and regressors were standardized to have a mean of 0 and a standard deviation of 1. The 1 by R vectors γ_{ik} and θ_k are random intercepts for subject and family respectively. These random intercepts accounted for baseline differences in each regional measurement between subjects and families. In order to account for intra-individual change, a random slope for time from baseline was included for each subject. δ_{ik} is the row vector of R of random slopes for subject i, and Z_{ijk} is the time from baseline value for subject i at time point j within family k. Finally, Σ is a R by R covariance matrix.

As with all Bayesian analyses, our model requires the user specify prior distributions for each model parameter. We experimented with several different prior distributions, and found our results were consistent over a range of priors. Each fixed effect β was assumed to be independently and identically distributed with a weak normal prior[4]:

$$\beta \sim Normal(0.0, 5.0) \ (2)$$

The covariance matrix, Σ, was constructed so that $\Sigma = diag(\sigma_e * \sigma_e)$ where σ_e is a vector of R error standard deviations with a cauchy prior[4,5]:

$$\sigma_e \sim cauchy(0.0, 2.5) \ (3)$$

It is important to understand that while this set of priors assumes that the regional measurement errors are independent, our model does not assume that the regional measurements themselves are independent. Rather, we use a simplification common to multivariate LME models[6] and assume that the regional data is independent conditional on the subject-level random effects:

$$\gamma_{ik} \sim Normal(0.0, D_\gamma) \text{ and } \delta_{ik} \sim Normal(0.0, D_\delta) \ (4)$$

where D_γ and D_δ are each R by R covariance matrices. Note that while these priors allow for regional correlations within intercepts and slopes, they do not allow for correlations between slopes and intercepts. While this is unlikely to be true for all biomarker measures, modeling the correlations between all the regional slopes and intercepts would require estimating a Rx2 by Rx2 covariance matrix. Without further

constraints, this would result in a large increase in the number of model parameters. This is something we choose to avoid given the relatively small number of time points available for each subject.

The variance and correlation components of D_γ and D_δ were given separate priors in order to eliminate any prior relationship between the two components[7,8]. The variance components used Cauchy priors:

$$\sigma_\gamma \sim cauchy(0.0, 2.5) \text{ and } \sigma_\delta \sim cauchy(0.0, 2.5) \text{ (5)}$$

where σ_γ and σ_δ are R length vectors of standard deviations for the subject intercept and slope parameters. The correlation components used LKJ Cholesky correlation priors[9,4]

$$L_\gamma \sim lkj\_corr\_cholesky(1.0) \text{ and } L_\delta \sim lkj\_corr\_cholesky(1.0) \text{ (6)}$$

where L_γ and L_δ are the Cholesky factorizations of the correlation matrices for the intercepts and slopes respectively. A value of 1.0 in the LKJ correlation prior implies a uniform prior over all correlation matrices[4,10]. Finally, the family level regional intercepts were assumed to be independent, so that:

$$\theta_k \sim Normal(0.0, diag(\sigma_\theta * \sigma_\theta)) \text{ (7)}$$

where σ_θ is a vector of R standard deviations:

$$\sigma_\theta \sim cauchy(0.0, 2.5) \text{ (8)}$$

We tested models where the family intercepts were correlated, but found little evidence for regional correlations at this level.

All model fitting was performed using Hamilton Markov chain Monte Carlo implemented in version 2.9.0 of the probabilistic programming environment Stan[11]. Our Stan model code is included below. Each model was run using eight independent chains consisting of 10,000 iterations after 10,000 warm-up samples. In order to account for autocorrelation within a chain, we limited analysis to every 10th sample. As a result, all inference was performed on 8,000 final samples. Convergence was assessed using the Gelman-Rubin $\hat{R}$ statistic[12,13]. $\hat{R}$ is a ratio of the within chain variance to the pooled between chain variance. At convergence this ratio should equal 1.0. In all of our models $\hat{R}$ was found to be acceptably close to 1.0 for every model parameter (Supplemental Figure 1).

Stan Model, adapted loosely from[14]:

```
data {
  int<lower=1> N;                     //Number of data points
  int<lower=1> nY;                    //Number of responses
  int<lower=1> nB;                    //Number of fixed effects
  vector[nY] y[N];                    //Matrix of responses
  vector[nB] X[N];                    //Fixed effects design matrix
  int<lower=1> nS;                    //Number of subjects
  int<lower=1,upper=nS> subj[N];      //Subject indicator
  vector[N] Z;                        //Subject time from baseline variable
  int<lower=1> nF;                    //Number of families
  int<lower=1,upper=nF> fam[N];       //Family indicator
}

parameters {
  matrix[nY,nB] beta;                 //Fixed effects coefficients
  matrix[nY,nS] gammaZ;               //Random normals needed to generate random intercepts for subject
  matrix[nY,nS] deltaZ;               //Random normals needed to generate random slopes for subject
  matrix[nY,nF] thetaZ;               //Random normals needed to generate random intercepts for family
  cholesky_factor_corr[nY] gL;        //Cholesky factorization of the correlation matrix for subject intercepts
  cholesky_factor_corr[nY] dL;        //Cholesky factorization of the correlation matrix for subject slopes
  vector<lower=0>[nY] eSigma;         //Error standard deviations
  vector<lower=0>[nY] gSigma;         //Standard deviations for random subject intercepts
  vector<lower=0>[nY] dSigma;         //Standard deviations for random subject slopes
```

```
    vector<lower=0>[nY] tSigma;              //Standard deviations for family intercepts
}

transformed parameters {
    matrix[nY,nS] gamma;                     //Coefficients for random subject intercepts
    matrix[nY,nS] delta;                     //Coefficients for random subject slopes
    matrix[nY,nF] theta;                     //Coefficients for random family intercepts
    gamma = diag_pre_multiply(gSigma,gL) * gammaZ;    //Implies gamma ~ Normal(0,Dg)
    delta = diag_pre_multiply(dSigma,dL) * deltaZ;    //Implies delta ~ Normal(0,Dd)
    theta = diag_matrix(tSigma) * thetaZ;             //Implies theta ~ Normal(0,Dt)
}

model {
    vector[nY] mu[N];

    //Priors
    gL ~ lkj_corr_cholesky(1.0);
    dL ~ lkj_corr_cholesky(1.0);
    to_vector(beta) ~ normal(0,5);
    to_vector(gammaZ) ~ normal(0,1);
    to_vector(deltaZ) ~ normal(0,1);
    to_vector(thetaZ) ~ normal(0,1);
    eSigma ~ cauchy(0,2.5);
    gSigma ~ cauchy(0,2.5);
    dSigma ~ cauchy(0,2.5);
    tSigma ~ cauchy(0,2.5);

    //Model predictions
    for (i in 1:N)
        mu[i] = beta*X[i] + gamma[,subj[i]] + delta[,subj[i]]*Z[i] + theta[,fam[i]];

    //Likelihood
    y ~ multi_normal(mu,diag_matrix(eSigma .* eSigma));
}
```

Supplemental Figure 1: Model Convergence measured with $\widehat{R}$
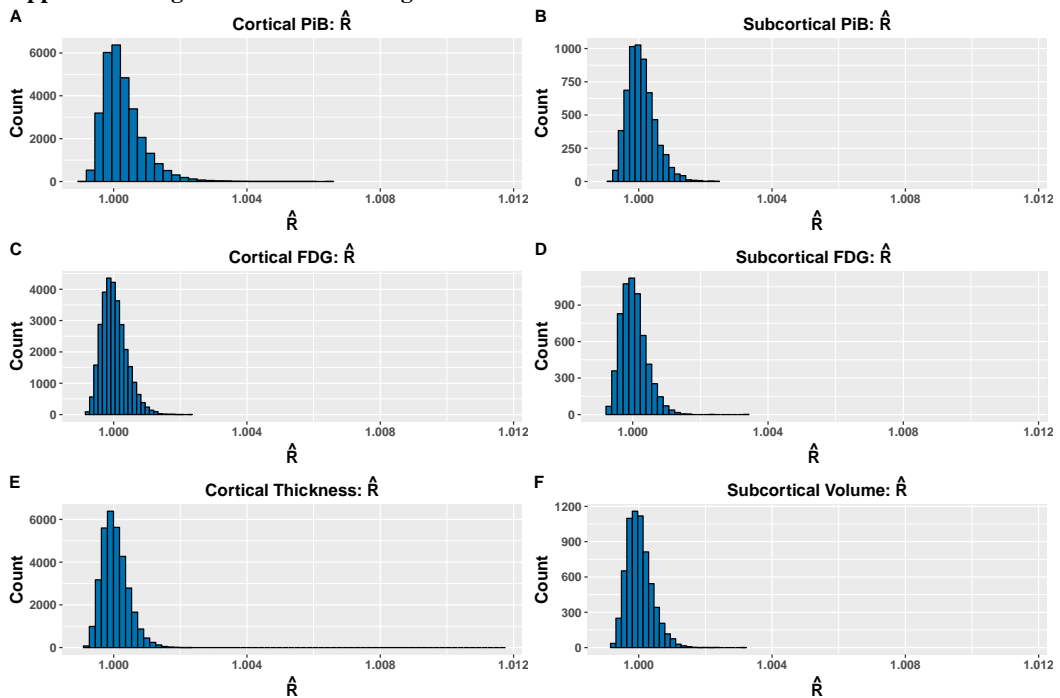
Supplemental Figure 1. The Gelman-Rubin $\hat{R}$ statistic[12,13] is a marker that at convergence should equal 1.0. In all of our models $\hat{R}$ was found to be acceptably close to 1.0 for every model parameter.

Online Interactive Models

An interactive tool created with the R package Shiny[15] is hosted online at https://dianspatial.shinyapps.io/dian_longitudinal_neuroimaging/. This application provides a more in-depth depiction of the statistical models and results than is possible in the main manuscript. The online application has five distinct tabs: Baseline Trends, Longitudinal Trends (default starting tab), Spatial Maps, Regional Comparisons, and Posterior Distributions. For optimal performance, please use a modern version of Chrome or Safari.

The ***Baseline Trends*** tab takes you to the regional cross-sectional estimates derived as part of the longitudinal model. It is possible to view cross-sectional estimates for all three modalities and all brain regions. This tab also allows the user to display posterior predictive intervals for a new participant at baseline within a new family. The ***Longitudinal Trends*** tab depicts the longitudinal model results for all modalities and regions in a similar manner to the data presented in Figure 1 of the main manuscript. The solid lines in the panel labeled "*Fit*" are model estimates for each subject. An option is present to display the actual data alongside the model fits. The panel labeled "*Estimated Rates*" depicts the annualized rate of change, with each dot representing an individual's estimate. The two lines in this panel are group estimates of rate of change from the overall model for this selected region. The panel labeled "*Estimated Rate Differences*" depicts differences in the rate of biomarker change between mutation carriers and non-carriers. For both *Baseline Trends* and *Longitudinal Trends* data figures are displayed with baseline EYO -29 to +10 to avoid inadvertently revealing mutation status at points on the extreme ends of the range where sampling is lower.

The ***Spatial Maps*** tab provides the ability to display regional model estimates on a rendered brain using the rgl package in R[16]. The interactive toolbox allows the user to specify a number of parameters including the modality, model parameter of interest, statistic (mean, median, or standard deviation), and color scale. The ***Regional Comparisons*** tab presents a grid that directly compares the rate of biomarker change between anatomical regions (e.g. comparing the rate of PiB accumulation at an EYO of -10 in precuneus and the inferior parietal cortex). The values in the matrix always represent a difference between the region listed in the row minus the region represented by the column. The ***Posterior Distributions*** tab depicts the posterior distributions of the model estimates. This distribution provides us with the summary value for a parameter as well as the ability to test significance. If the 99% equal-tailed credible intervals do not overlap 0, then we consider the model parameter to be significant.

Supplementary Table 1: Cortical Regional Timing of Biomarker Abnormality

Region	PiB EYO	FDG EYO	MRI EYO	PiB EYO$_{Adj}$*	FDG EYO$_{Adj}$*	MRI EYO$_{Adj}$*
Caudal Anterior Cingulate	-20·0			-17·2		
Caudal Middle Frontal	-19·3	-17·4	-2·8	-16·5	-14·6	0·3
Cuneus	-2·5		-4·7	-0·1		-0·7
Entorhinal Cortex			-1·8			0·9
Frontal Pole	-18·3			-14·9		
Fusiform Gyrus	-17·1		-5·1	-9·8		-1·5
Inferior Parietal	-20·1	-12·4	-10·6	-17·8	-9·2	-7·2
Inferior Temporal	-19·7		-3·5	-16·8		-0·3
Insula	-18·6		-3·1	-15·3		-0·3
Isthmus Cingulate	-20·2		-3·0	-17·8		-0·4
Lateral Occipital	-20·1		-7·2	-17·8		-4·7
Lateral Orbital Frontal	-19·6			-17·0		
Lingual Gyrus	-17·9		-8·8	-2·4		-5·6
Medial Orbital Frontal	-21·2		2·3	-19·6		5·1
Middle Temporal Gyrus	-20·5		-5·2	-18·1		-2·7
Paracentral Gyrus	-19·9			-17·5		
Parahippocampus			-9·8			-6·7
Pars Opercularis	-20·7	-13·6	-5·1	-18·3	-8·8	-2·8
Pars Orbitalis	-17·1			-14·8		
Pars Triangularis	-19·9		0·0	-17·4		3·0
Pericalcarine	-20·0			-17·6		
Posterior Cingulate	-21·0			-18·6		
Postcentral Gyrus	-20·6		-2·3	-18·3		1·1
Precentral Gyrus	-18·0		0·0	-14·5		3·1
Precuneus	-22·2	-18·8	-13	-19·8	-16·5	-10·0
Rostral Anterior Cingulate	-20·4			-17·6		
Rostral Middle Frontal	-20·3			-18·1		
Banks Superior Temporal Sulcus	-18·7	-18·0	-11·5	-15·8	-15·6	-6·8
Superior Frontal	-19·0	-15·1	0·8	-16·6		3·0
Superior Parietal	-20·2	-14·9	-9·1	-17·8		-5·7
Superior Temporal	-20·1		-5·6	-17·9		-2·6
Supramarginal Gyrus	-20·1	-2·8	-6·9	-17·7	0·7	-3·6
Temporal Pole	-15·1			-1·5		
Transverse Temporal	-17·0		-3·0	-13·3		0·2

* See Adjusting EYO by Known Dementia Onsets section below for explanation of EYO$_{Adj}$

Supplementary Table 2: Subcortical Regional Timing of Biomarker Abnormality

Region	PiB EYO	FDG EYO	MRI EYO	PiB EYO$_{Adj}$*	FDG EYO$_{Adj}$*	MRI EYO$_{Adj}$*
Nucleus Accumbens	-22·2		-8·0	-20·8		-3·0
Amygdala			-0·5			2·8
Caudate	-16·4		3·6	-0·7		5·9
Hippocampus			-7·1			-3·7
Pallidum						
Putamen	-17·0			-9·4		
Thalamus						

* See Adjusting EYO by Known Dementia Onsets section below for explanation of EYO$_{Adj}$

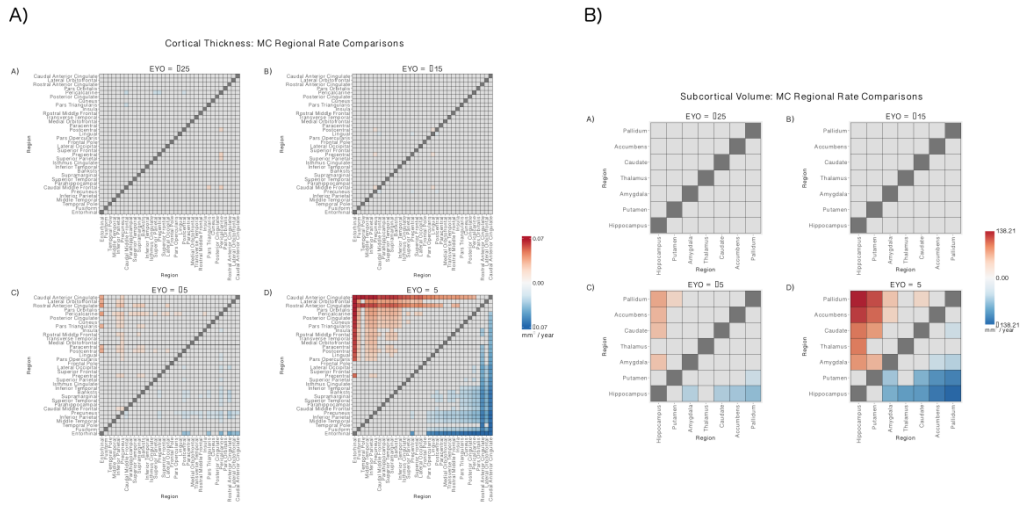**Regional Comparisons of Biomarker Accumulation**

Supplemental Figure 2
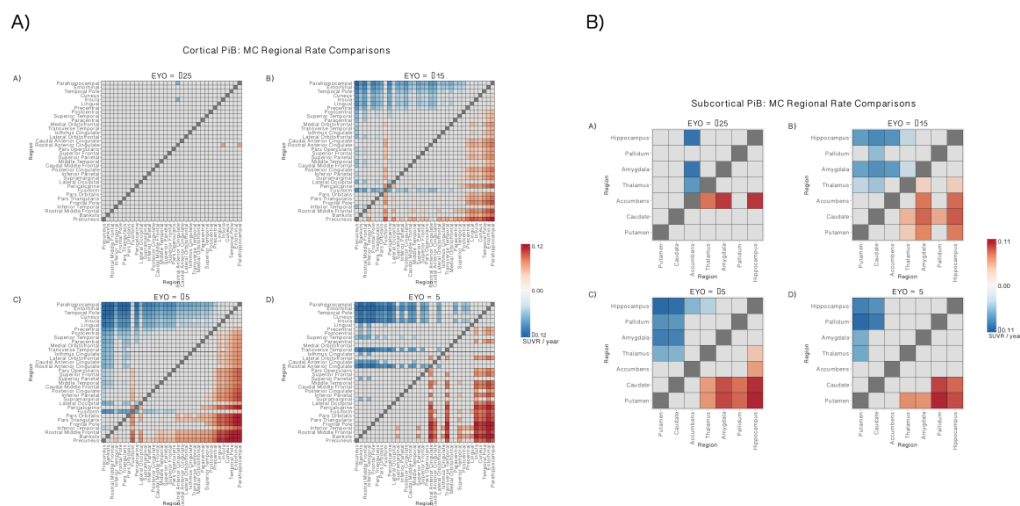
Supplemental Figure 2: Panel 2A presents regional pair-wise comparisons in rates of beta-amyloid deposition at EYOs of -25, -15, -5 and +5. The color-coding on the figures represents the estimated differences between regional rates. Only comparisons whose 99% credible intervals do not overlap 0 are shown. The comparison is always the region listed in the row minus the region listed in the column. Supplemental Figure 2B compares similarly compares subcortical accumulation of beta-amyloid.

Supplemental Figure 3
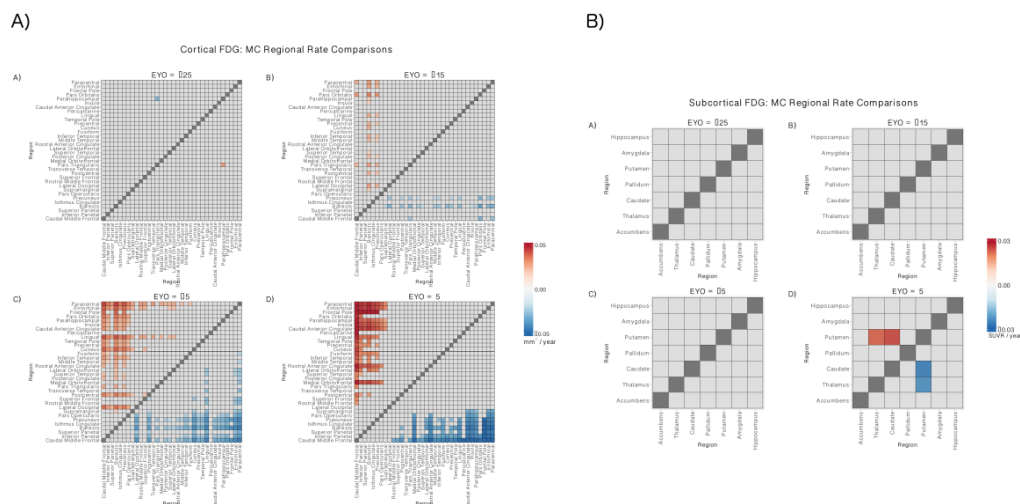
Supplemental Figure 3: Differences in longitudinal rates of FDG changes in A) cortical and B) subcortical regions respectively.

Supplemental Figure 4: Differences in longitudinal rates of change in A) cortical thickness and B) subcortical volume respectively.

Movies Illustrating Rates of Change

To further illustrate patterns of regional change we examined our data at the voxel-wise level. PET data were partial volume corrected using a region-bases voxel-wise (RBV)[17] approach which is a voxel-wise extension of the regional spread function technique implemented on our ROI analyses. Data were smoothed on the cortical surface using a 10 mm kernel. Our linear mixed-effects models were then fit at a voxel-wise level using the R statistical software package lme4[18] (https://github.com/lme4/lme4). The model estimates were then used to compose the movies included with the main body of the manuscript. The upper portion of the movie depicts the rate of change of the biomarker (PiB, FDG, MRI) across EYO (from -25 to +10) in mutation carriers. The bottom portion of the movie figure depicts the total biomarker levels at each EYO for mutation carriers. This is derived from integrating the rate of change and adding it to the estimated value of a mutation carrier at an EYO of -25 and time zero.

Movie 1: Voxel-wise change for beta-amyloid deposition by PiB PET in mutation carriers. The top panel of the figure shows the rate of change at each EYO. The bottom panel depicts the total biomarker levels at each EYO for mutation carriers derived by integrating the rate of change and adding it to the baseline value of a mutation carrier at an EYO of -25 and time zero.

Movie 2: Voxel-wise change in FDG PET uptake in mutation carriers. The top panel of the figure shows the rate of change at each EYO. The bottom panel depicts the total biomarker levels at each EYO for mutation carriers derived by integrating the rate of change and adding it to the baseline value of a mutation carrier at an EYO of -25 and time zero.

Movie 3: Voxel-wise change in cortical thickness by MRI in mutation carriers The top panel of the figure shows the rate of change at each EYO. The bottom panel depicts the total biomarker levels at each EYO for mutation carriers derived by integrating the rate of change and adding it to the baseline value of a mutation carrier at an EYO of -25 and time zero.

Adjusting EYO by Known Dementia Onsets

Prior analyses examining ADAD have used self-report of parental age of onset[19] or mutation specific[20] estimates of disease onset. To be consistent with prior work in the field, the current analyses utilize these two measures to define an individual's estimated years to symptom onset (EYO). However, the longitudinal clinical assessments given as part of DIAN provide the ability to relate expected times of dementia onset to the point where clinicians note the first departure from clinical normality. To do this we examined those mutation carriers who went from cognitive normality at baseline, denoted by a CDR[21]=0, to CDR>0. The first point where an individual reached a CDR>0 was considered their decline age (DA). The relationship between the individuals' DA and parental estimated age of onset (EAO) was calculated using a bivariate linear errors-in-variables modeling using the R package "levi"[22].

As seen in the Supplemental Figure 5, individuals regularly show a clinical decline (CDR >0) before their expected parental EAO. The most likely explanation is that when individuals are reporting the dementia onset of a family member they are reporting a cognitive impairment that is more sever than a CDR 0·5. The model fit provides a way to adjust calculate a DA in both carriers and non-carriers to capture this early clinical decline. This calculated DA can be used to compute an adjusted EYO (EYO$_{adj}$). All analytical models were re-run using this EYO$_{adj}$. The significant findings using EYO$_{adj}$ are highly similar to EYO calculated using the standard mutation or parental EAO. Not surprising given the model fit, the emergence of biomarker changes (Supplemental Table 1) happens in closer approximation to an EYO$_{adj}$ of 0 (e.g. Precuneus PiB emergence shifting from an EYO -22·2 to EYO$_{adj}$ of -19·8). The spatial patterns and relative temporal ordering between modalities are preserved (Supplemental Figure 6).

Supplemental Figure 5: Relating EYO to Decline Age

Age at Onset Estimation

$$DA = EAO * 1.16 + -10.62$$
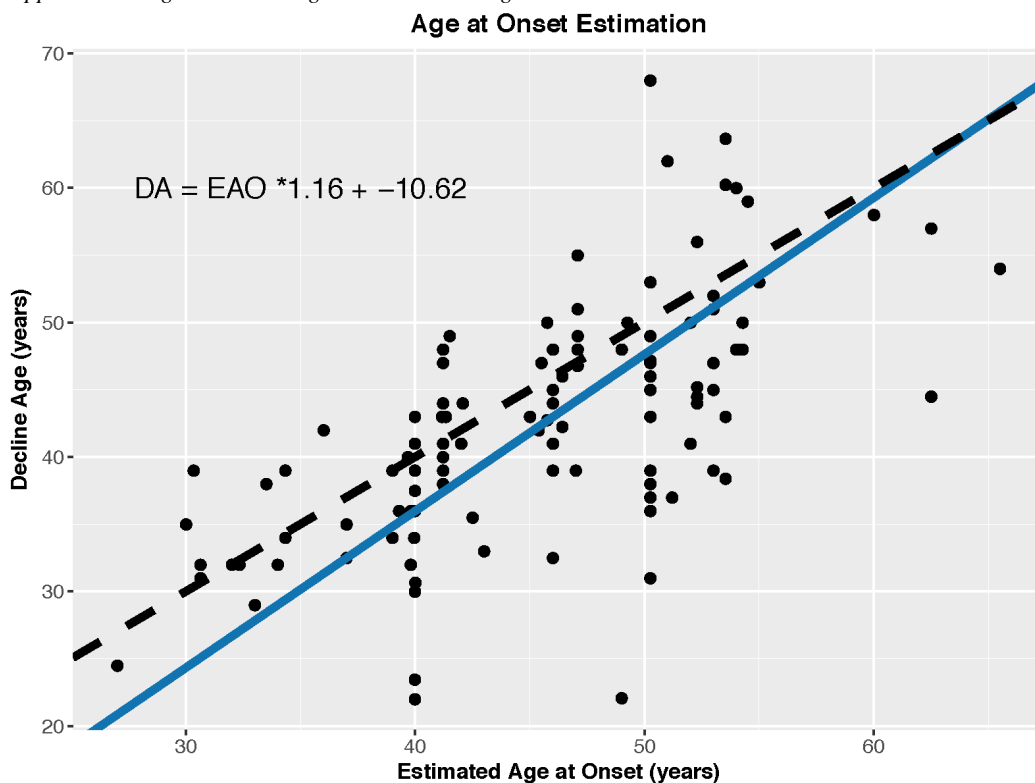
Supplemental Figure 5. The relational between estimated age of onset and actual decline age (first visit CDR >0) calculated using a bivariate linear errors-in-variables modeling using the R package "levi"[22]. The blue line represents the model fit while the black dashed line is the identity line.

Supplemental Figure 6.
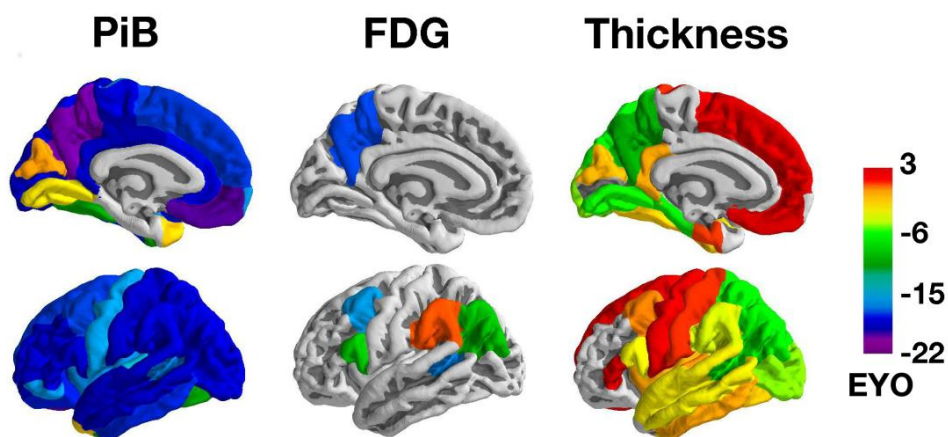
Supplemental Figure 6: Emergence of neuroimaging biomarkers. The color scale represents the first point in the disease using the adjusted EYO (EYO$_{adj}$) where rates of biomarker change in that cortical region are significantly different between mutation carriers and non-carriers. As with the results presented in Figure 2 in the main text, there is a temporal evolution where increased amyloid deposition precedes hypometabolism that in turn is followed by cortical thinning.

Dutch and Flemish Mutation Carriers

Autosomal dominant mutation carriers of the APP Dutch (Glu693Gln) and Flemish (Ala692Gly) mutations often present with predominant vascular Aβ deposition, with diffuse plaques in the parenchymal tissue, cerebral hemorrhage, and cerebral amyloid angiopathy (CAA).[23] This Aβ can be problematic for PET imaging and these phenotypes may also have additional vascular contributions to the progression of their disease.[24] For these reasons the main analyses excluded all individuals from families of either mutation. We additionally ran all models including these two individuals with families with Flemish mutations twenty-one individuals with the Dutch mutation. Results were highly consistent with those presented in the main text.

Dutch Glu693Gln mutation
http://www.molgen.vib-ua.be/ADMutations/Default.cfm?MT=1&ML=0&Page=PublicationsByMut&ID=153

Flemish Ala692Gly mutation
http://www.molgen.vib-ua.be/ADMutations/Default.cfm?MT=1&ML=0&Page=PublicationsByMut&ID=56

Obtaining DIAN Data

Data from the DIAN project can be requested freely by researchers at the following website
https://dian.wustl.edu/our-research/observational-study/dian-observational-study-investigator-resources/

Movie Legends

Movie 1: Voxel-wise change for beta-amyloid deposition by PiB PET in mutation carriers. The top panel of the figure shows the rate of change at each EYO. The bottom panel depicts the total biomarker levels at each EYO for mutation carriers derived by integrating the rate of change and adding it to the baseline value of a mutation carrier at an EYO of -25 and time zero.

Movie 2: Voxel-wise change in FDG PET uptake in mutation carriers. The top panel of the figure shows the rate of change at each EYO. The bottom panel depicts the total biomarker levels at each EYO for mutation carriers derived by integrating the rate of change and adding it to the baseline value of a mutation carrier at an EYO of -25 and time zero.

Movie 3: Voxel-wise change in cortical thickness by MRI in mutation carriers. The top panel of the figure shows the rate of change at each EYO. The bottom panel depicts the total biomarker levels at each EYO for mutation carriers derived by integrating the rate of change and adding it to the baseline value of a mutation carrier at an EYO of -25 and time zero.

References

1. Fitzmaurice GM, Laird NM, Ware JH. *Applied Longitudinal Analysis*. 2nd ed. Wiley; 2011.
2. Bernal-Rusiel JL, Greve DN, Reuter M, Fischl B, Sabuncu MR. Statistical analysis of longitudinal neuroimage data with Linear Mixed Effects models. *Neuroimage*. 2013;66:249-260. doi:10.1016/j.neuroimage.2012.10.065.
3. Bernal-Rusiel JL, Reuter M, Greve DN, Fischl B, Sabuncu MR. Spatiotemporal linear mixed effects modeling for the mass-univariate analysis of longitudinal neuroimage data. *Neuroimage*. 2013;81:358-370. doi:10.1016/j.neuroimage.2013.05.049.
4. Team SD. Stan Modeling Language Users Guide and Reference Manual, Version 2.14.0. 2016.
5. Gelman A. Prior distributions for variance parameters in hierarchical models(Comment on Article by Browne and Draper). *Bayesian Anal*. 2006;1(3):515-534. doi:10.1214/06-BA117A.
6. Verbeke G, Fieuws S, Molenberghs G, Davidian M. The analysis of multivariate longitudinal data: a review. *Stat Methods Med Res*. 2014;23(1):42-59. doi:10.1177/0962280212445834.
7. Barnard J, McCulloch R, Meng XL. Modeling covariance matrices in terms of standard deviations and correlations, with application to shrinkage. *Stat Sin*. 2000;10(4):1281-1311.
8. Alvarez I, Niemi J, Simpson M. Bayesian inference for a covariance matrix. August 2014.
9. Lewandowski D, Kurowicka D, Joe H. Generating random correlation matrices based on vines and extended onion method. *J Multivar Anal*. 2009;100(9):1989-2001. doi:10.1016/j.jmva.2009.04.008.
10. Dauwels J, Vialatte F, Cichocki A. Diagnosis of Alzheimer's Disease from EEG Signals: Where Are We Standing? *Curr Alzheimer Res*. 2010;999(999):1-19. doi:10.2174/1567210204558652050.
11. Carpenter B, Lee D, Brubaker MA, et al. Stan: A Probabilistic Programming Language. *J Stat Softw*. 2016.
12. Gelman A, Rubin DB. Inference from Iterative Simulation Using Multiple Sequences. *Stat Sci*. 1992;7(4):457-472.
13. Brooks SP, Gelman A. General Methods for Monitoring Convergence of Iterative Simulations. *J Comput Graph Stat*. 1998;7(4):434-455. doi:10.1080/10618600.1998.10474787.
14. Sorensen T, Vasishth S. Bayesian linear mixed models using Stan: A tutorial for psychologists, linguists, and cognitive scientists. June 2015. doi:10.20982/tqmp.12.3.p175.
15. Chang W, Cheng J, Allaire J, Xie Y, McPherson J. Shiny: Web Application Framework for R. 2016.
16. Adler D, Murdoch D, Nenadic O, et al. RGL: 3D Visualization Using OpenGL. 2016.
17. Thomas BA, Erlandsson K, Modat M, et al. The importance of appropriate partial volume correction for PET quantification in Alzheimer's disease. *Eur J Nucl Med Mol Imaging*. 2011;38(6):1104-1119. doi:10.1007/s00259-011-1745-9.
18. Bates D, Mächler M, Bolker B, Walker S. Fitting Linear Mixed-Effects Models Using lme4. *J Stat Softw*. 2015;67(1):1-48. doi:10.18637/jss.v067.i01.
19. Bateman RJ, Xiong C, Benzinger TLS, et al. Clinical and biomarker changes in dominantly inherited Alzheimer's disease. *N Engl J Med*. 2012;367(9):795-804. doi:10.1056/NEJMoa1202753.
20. Ryman DC, Acosta-Baena N, Aisen PS, et al. Symptom onset in autosomal dominant Alzheimer disease: a systematic review and meta-analysis. *Neurology*. 2014;83(3):253-260. doi:10.1212/WNL.0000000000000596.
21. Morris JC. The Clinical Dementia Rating (CDR): Current version and scoring rules. *Neurology*. 1993;43(11):2412-2414.
22. Leonard D. Estimating a bivariate linear relationship. *Bayesian Anal*. 2011;6(4):727-754. doi:10.1214/11-BA627.
23. Guerreiro RJ, Gustafson DR, Hardy J. The genetic architecture of Alzheimer's disease: beyond APP, PSENs and APOE. *Neurobiol Aging*. 2012;33(3):437-456. doi:10.1016/j.neurobiolaging.2010.03.025.
24. van Opstal AM, van Rooden S, van Harten T, et al. Cerebrovascular function in presymptomatic and symptomatic individuals with hereditary cerebral amyloid angiopathy: a case-control study. *Lancet Neurol*. 2017;16(2):115-122. doi:10.1016/S1474-4422(16)30346-5.

A) Precuneus PiB

B) Precuneus PiB Change

C) Precuneus MC – NC PiB Change

D) Precuneus FDG

E) Precuneus FDG Change

F) Precuneus MC – NC FDG Change

G) Precuneus Thickness

H) Precuneus Thickness Change

I) Precuneus MC – NC Thickness Change

Figure 2 EYO

A) PiB   EYO = -25   EYO = -15   EYO = -5   EYO = 5

0.16
0.00
-0.16
SUVR/year

B) FDG

0.05
0.00
-0.05
SUVR/year

C) Thickness

0.75
0.00
-0.75
mm/year
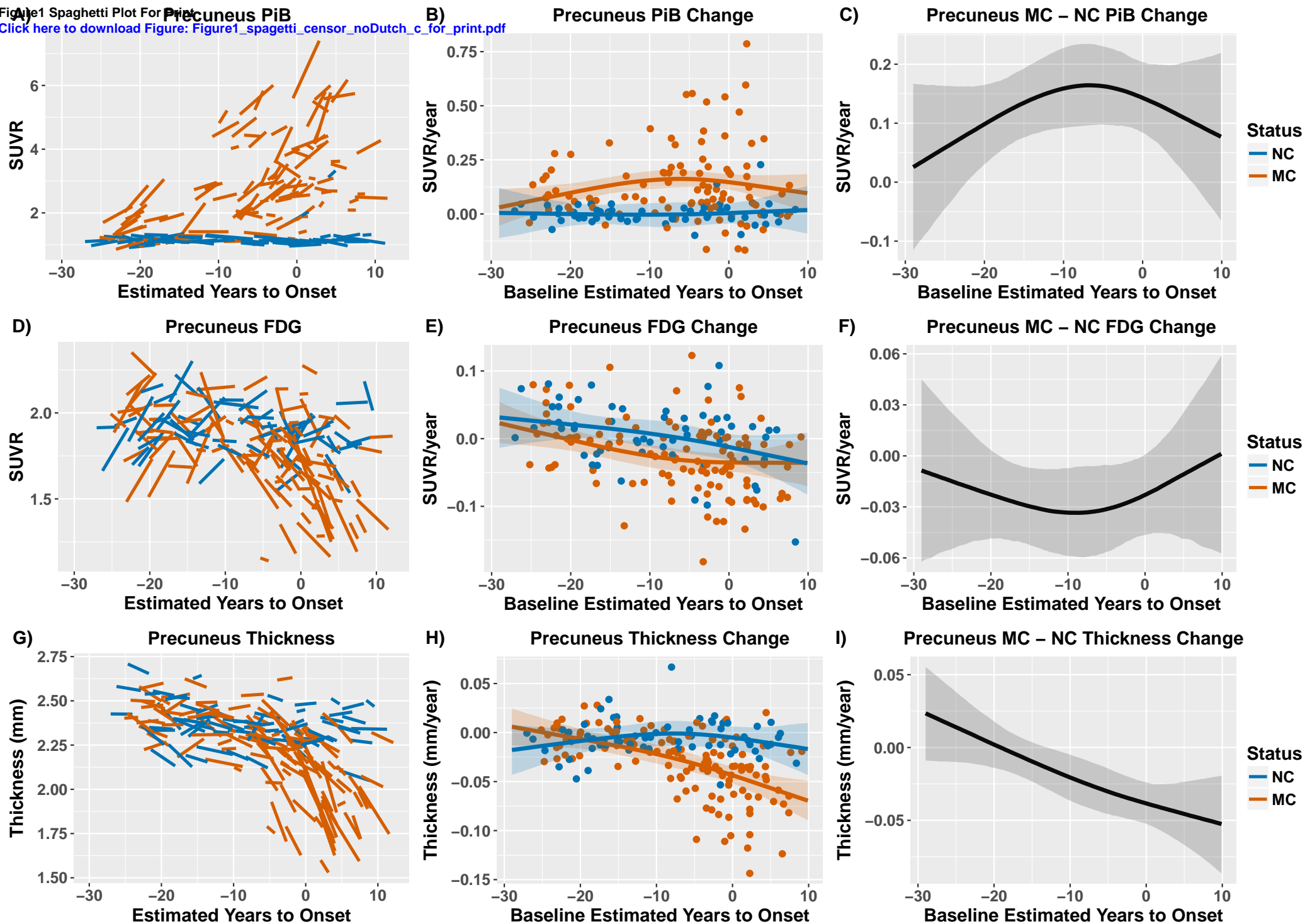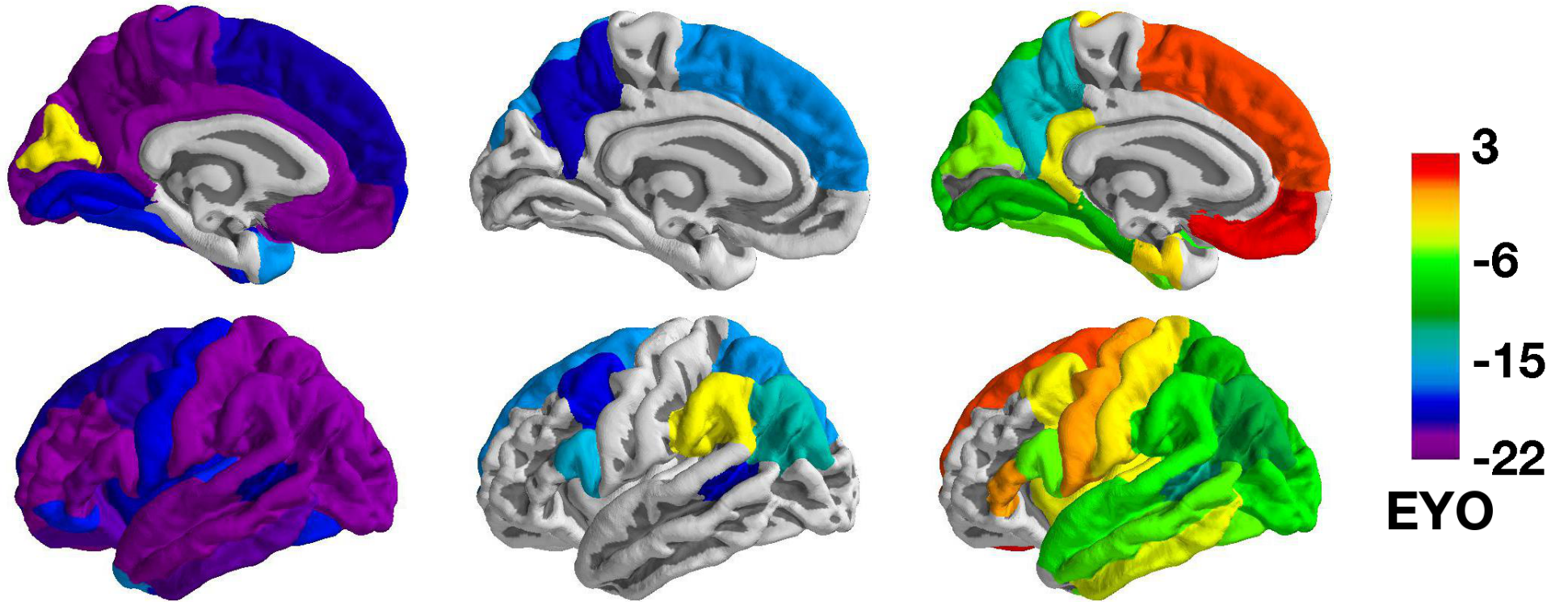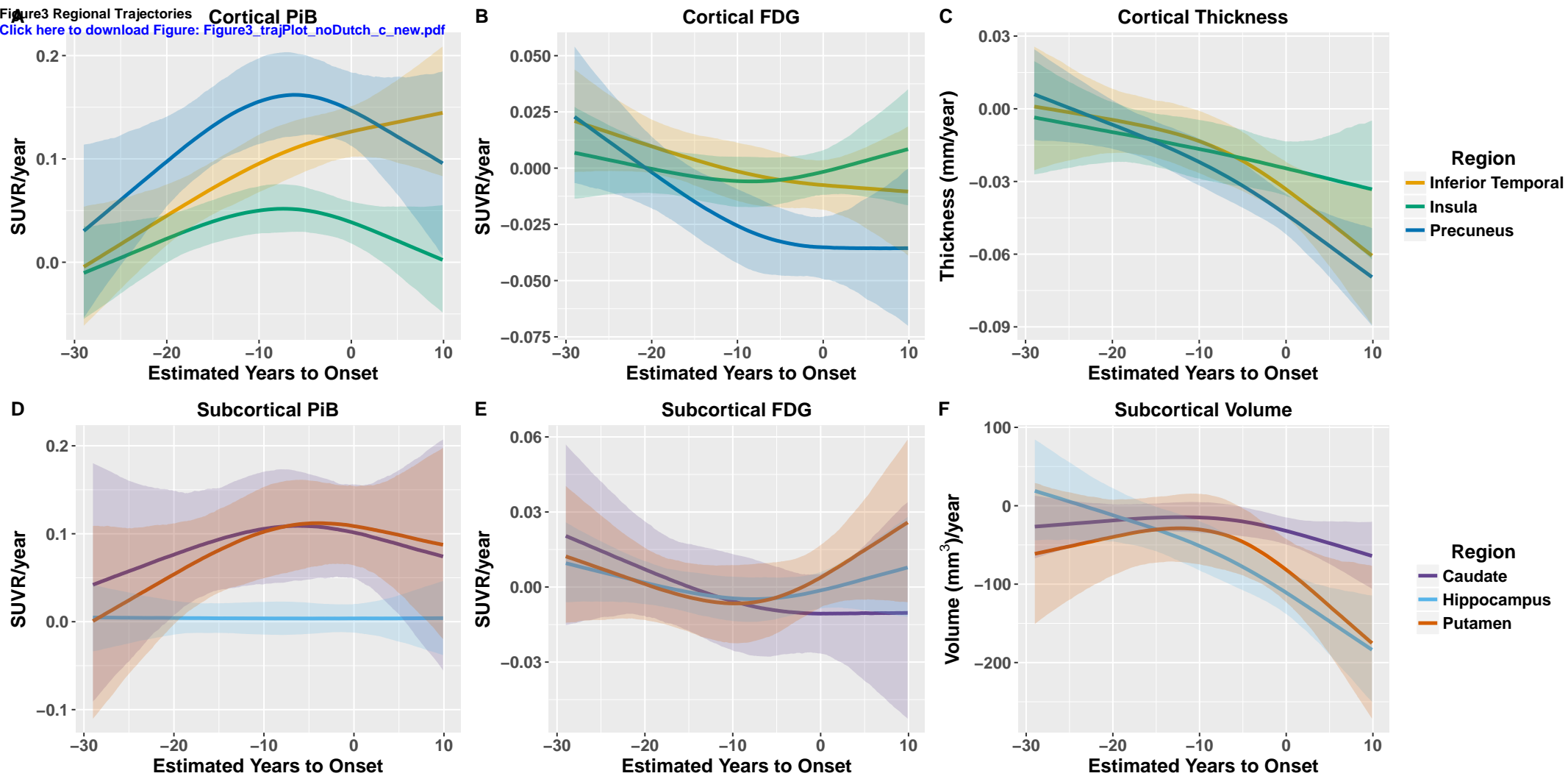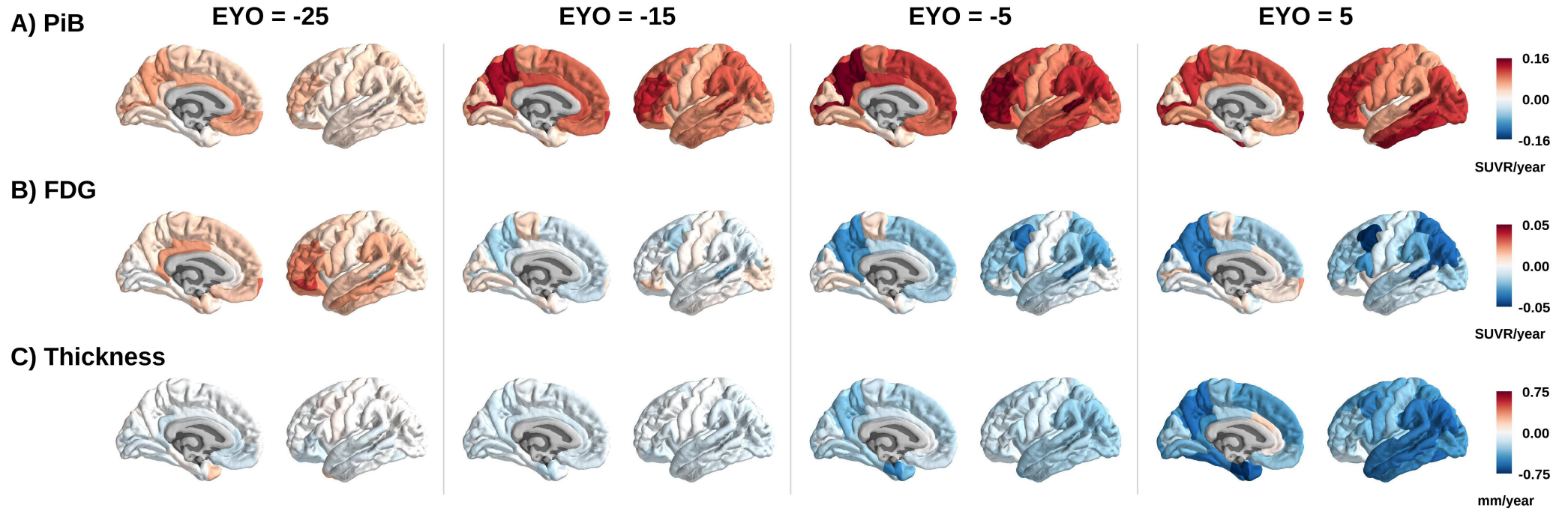
Video 1 PIB

Click here to download Video: Movie1_pibRateRdBuMovieRBVDutch.mp4

Video 2 FDG

[Click here to download Video: Movie2_fdgRateRdBuMovieRBVDutch.mp4](#)

Video 3 MRI
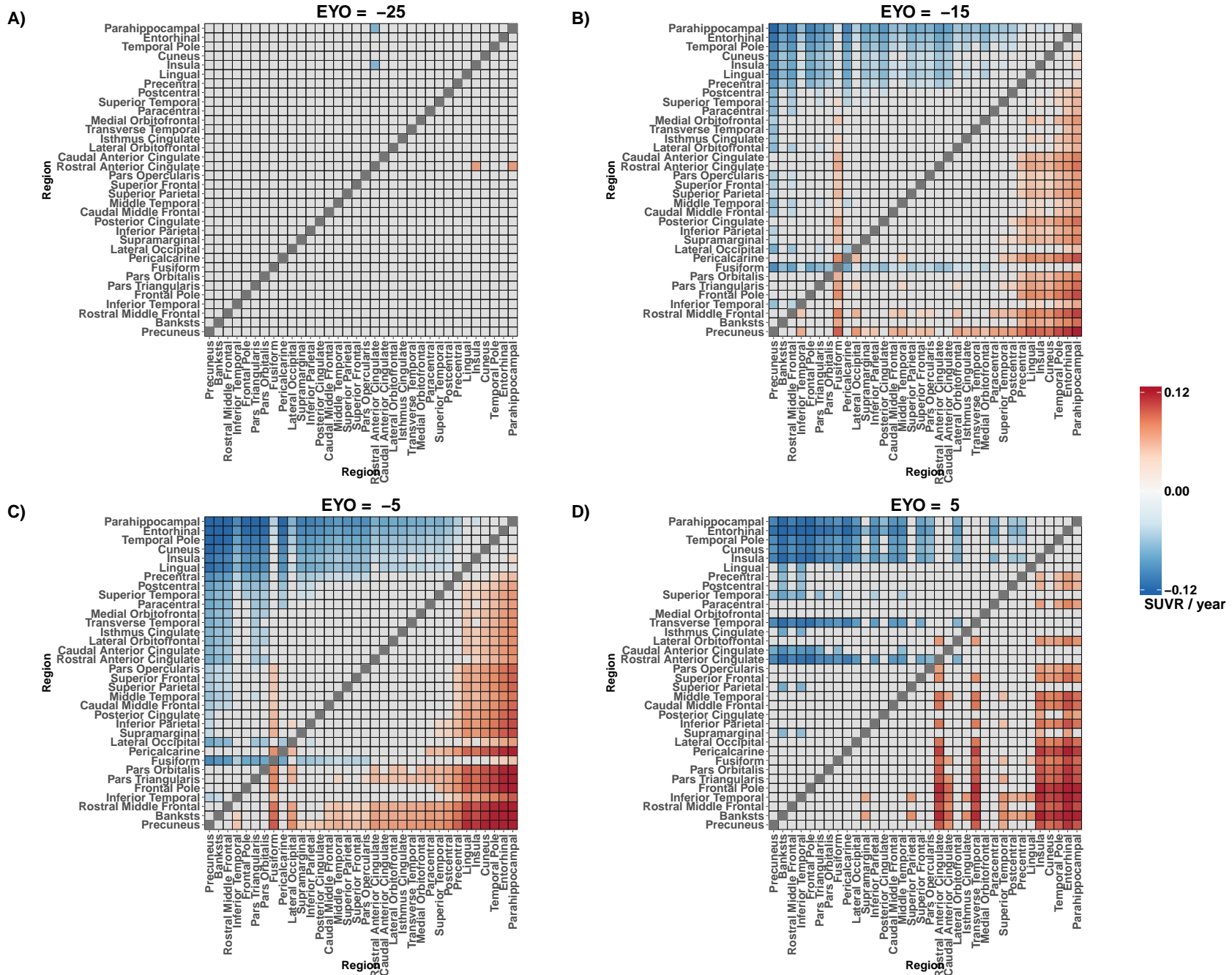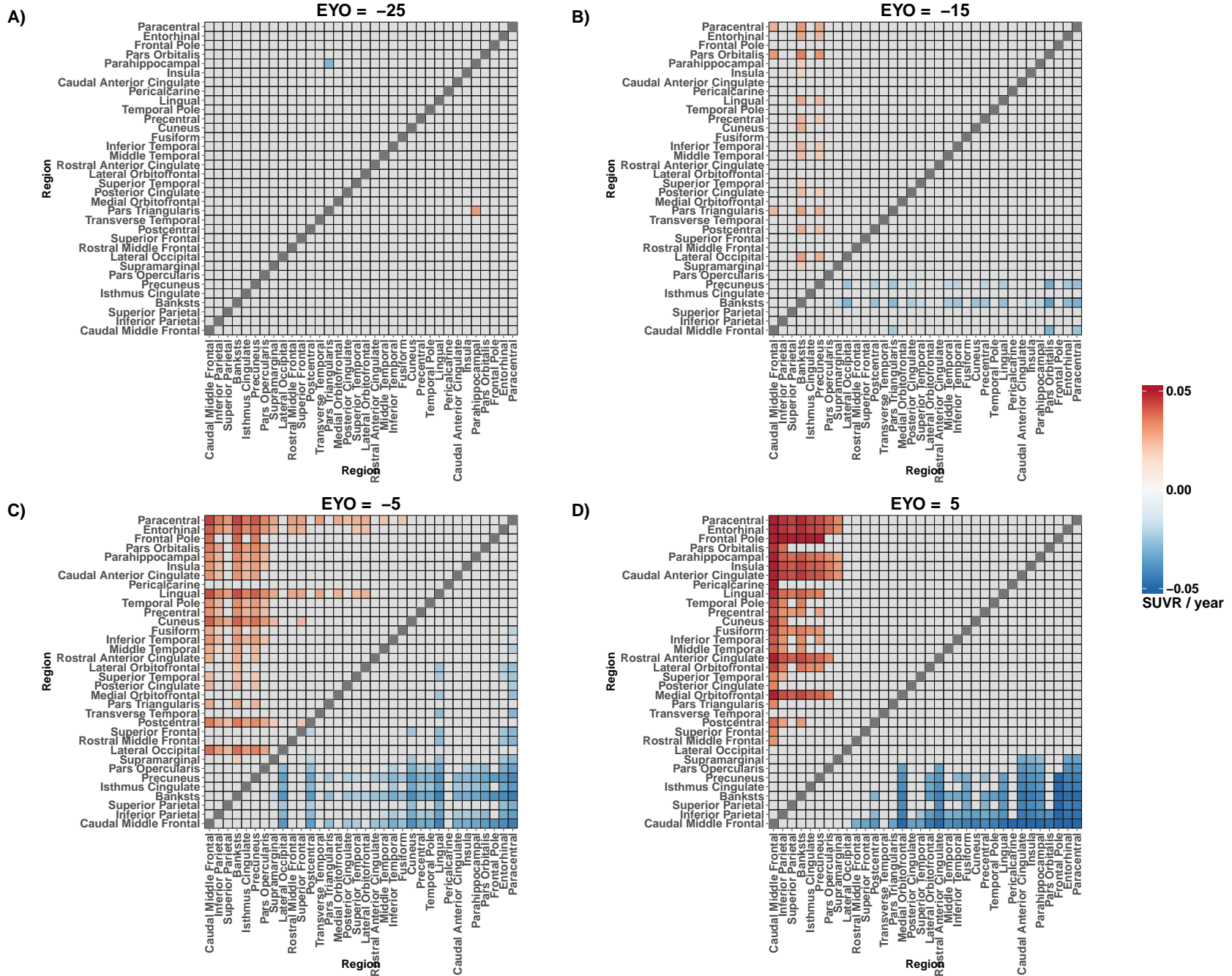**Click here to download Video: Movie3_thicknessRateRdBuMovieDutch.mp4**

Cortical PiB: MC Regional Rate Comparisons

Subcortical PiB: MC Regional Rate Comparisons
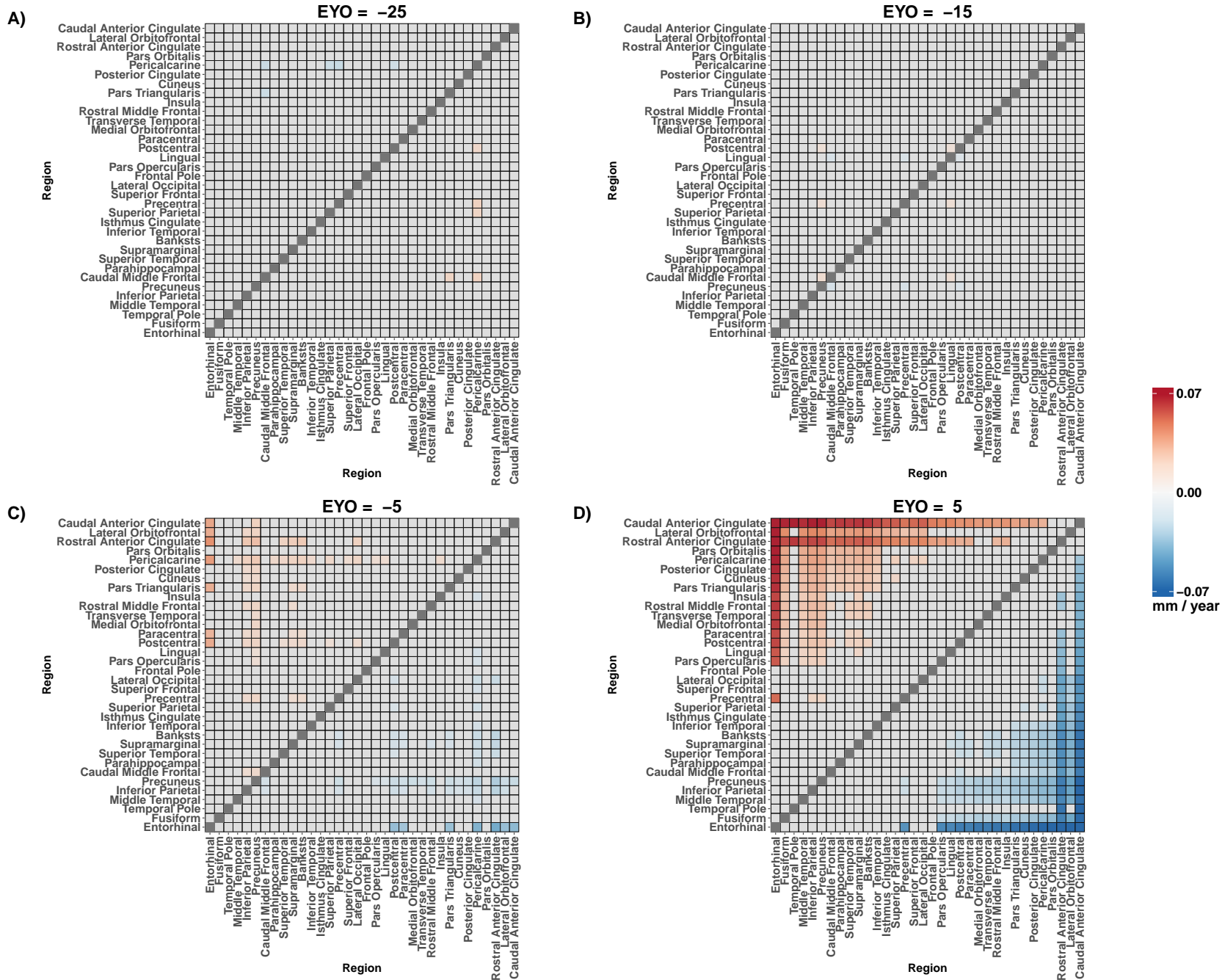
Cortical FDG: MC Regional Rate Comparisons

Subcortical FDG: MC Regional Rate Comparisons
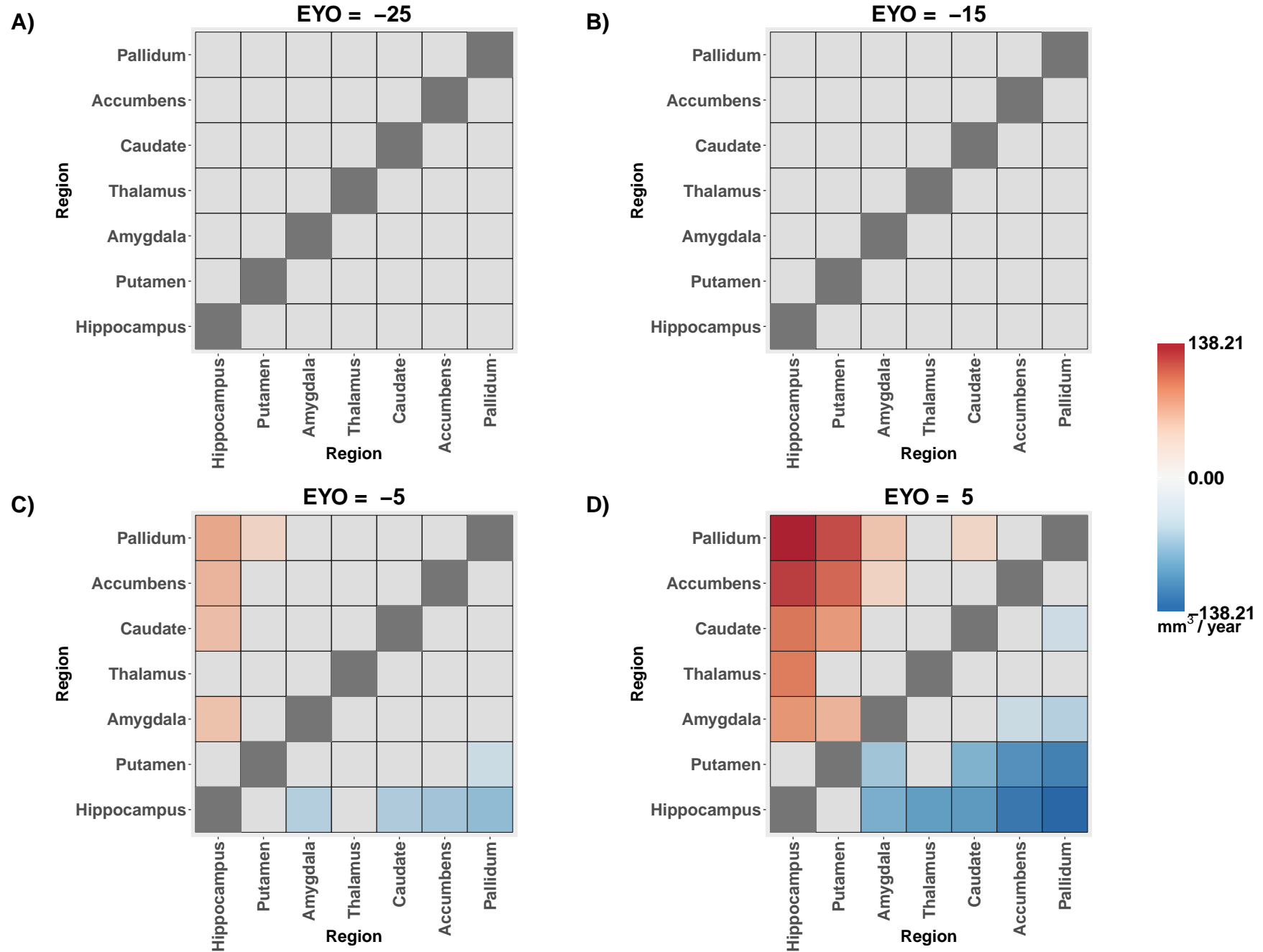
Cortical Thickness: MC Regional Rate Comparisons

Subcortical Volume: MC Regional Rate Comparisons

STROBE Statement—checklist of items that should be included in reports of observational studies

	Item No.	Recommendation	Page No.	Relevant text from manuscript
Title and abstract	1	(*a*) Indicate the study's design with a commonly used term in the title or the abstract	Title Page	Longitudinal study
		(*b*) Provide in the abstract an informative and balanced summary of what was done and what was found	Abstract Page	
Introduction				
Background/rationale	2	Explain the scientific background and rationale for the investigation being reported	1	
Objectives	3	State specific objectives, including any prespecified hypotheses	1-2	Our current work compares rates of biomarker change in a large population of mutation carriers (MC) and non-carriers (NC) throughout the entire brain. In this way we can visualize when pathology biomarkers first emerge and how they spread throughout the course of the disease.
Methods5				
Study design	4	Present key elements of study design early in the paper	2-5	Participants and Statistics Section
Setting	5	Describe the setting, locations, and relevant dates, including periods of recruitment, exposure, follow-up, and data collection	2	Participant section
Participants	6	(*a*) *Cohort study*—Give the eligibility criteria, and the sources and methods of selection of participants. Describe methods of follow-up *Case-control study*—Give the eligibility criteria, and the sources and methods of case ascertainment and control selection. Give the rationale for the choice of cases and controls *Cross-sectional study*—Give the eligibility criteria, and the sources and methods of selection of participants	2	All participants with genetic, clinical, and neuroimaging data that passed quality control from the tenth semiannual data freeze were included in the analyses.
		(*b*) *Cohort study*—For matched studies, give matching criteria and number of exposed and unexposed *Case-control study*—For matched studies, give matching criteria and the number of controls per case		
Variables	7	Clearly define all outcomes, exposures, predictors, potential confounders, and effect modifiers.	4-5	Statistics Section

		Give diagnostic criteria, if applicable		
Data sources/ measurement	8*	For each variable of interest, give sources of data and details of methods of assessment (measurement). Describe comparability of assessment methods if there is more than one group	2-4	Modality specific data paragraphs
Bias	9	Describe any efforts to address potential sources of bias	4-5	Statistics paragraphs as well as in depth material in the supplemental material
Study size	10	Explain how the study size was arrived at	2	All participants with genetic, clinical, and neuroimaging data that passed quality control from the tenth semiannual data freeze were included in the analyses.

Quantitative variables	11	Explain how quantitative variables were handled in the analyses. If applicable, describe which groupings were chosen and why	2-5	Participants section and stats section
Statistical methods	12	(*a*) Describe all statistical methods, including those used to control for confounding	4-5	In depth statistical section and supplemental material
		(*b*) Describe any methods used to examine subgroups and interactions	4-5	Described as part of the linear mixed effects model
		(*c*) Explain how missing data were addressed	4-5	Described as part of the linear mixed effects model
		(*d*) *Cohort study*—If applicable, explain how loss to follow-up was addressed *Case-control study*—If applicable, explain how matching of cases and controls was addressed *Cross-sectional study*—If applicable, describe analytical methods taking account of sampling strategy	Supplemental	In the supplemental material we discuss how our statistics are robust to different numbers of time points and unequal sampling.
		(*e*) Describe any sensitivity analyses	Supplemental Material	
Results				
Participants	13*	(a) Report numbers of individuals at each stage of study—eg numbers potentially eligible, examined for eligibility, confirmed eligible, included in the study, completing follow-up, and analysed	2	All participants with genetic, clinical, and neuroimaging data that passed quality control from the tenth semiannual data freeze were included in the analyses. Analyses excluded families with the Dutch and Flemish Mutation as these APP mutations often present with predominant cerebral amyloid angiopathy and diffuse Aβ plaques.
		(b) Give reasons for non-participation at each stage	2	We only excluded due to these two mutations.
		(c) Consider use of a flow diagram		
Descriptive data	14*	(a) Give characteristics of study participants (eg demographic, clinical, social) and information on exposures and potential confounders	13	Demographics table
		(b) Indicate number of participants with missing data for each variable of interest	13	Demoraphics table
		(c) *Cohort study*—Summarise follow-up time (eg, average and total amount)	13	Demoraphics table
Outcome data	15*	*Cohort study*—Report numbers of outcome events or summary measures over time	13	Demoraphics table
		Case-control study—Report numbers in each exposure category, or summary measures of exposure		
		Cross-sectional study—Report numbers of outcome events or summary measures		

Main results	16	(*a*) Give unadjusted estimates and, if applicable, confounder-adjusted estimates and their precision (eg, 95% confidence interval). Make clear which confounders were adjusted for and why they were included	Figures, online interactive	We provide an online resource to look at the actual estimates for every parameter for every region
		(*b*) Report category boundaries when continuous variables were categorized		
		(*c*) If relevant, consider translating estimates of relative risk into absolute risk for a meaningful time period		

Continued on next page

Other analyses	17	Report other analyses done—eg analyses of subgroups and interactions, and sensitivity analyses		

Discussion

Key results	18	Summarise key results with reference to study objectives	8	AD is not static but possesses dynamism in terms of what pathological processes first appear, and how such pathology propagates throughout the brain. As dementia onset is predictable in ADAD, it provides an elegant model with which to examine pathological staging. Characterizing the spatial and temporal spread of pathology provides insight to the pathophysiology of the disease, informs how neuroimaging could aid optimal subject recruitment in clinical trials, and is critical to measure the efficacy of interventions on longitudinal biomarker measurements.
Limitations	19	Discuss limitations of the study, taking into account sources of potential bias or imprecision. Discuss both direction and magnitude of any potential bias	10	Almost all of page 10 considers limitations of the study
Interpretation	20	Give a cautious overall interpretation of results considering objectives, limitations, multiplicity of analyses, results from similar studies, and other relevant evidence	10	The discussion takes pains to present work in a cautions manner. For example "This means results at the edges of the EYO range where outliers have disproportional influence must be interpreted with care. As the DIAN study gains more time points longitudinal estimates will be improved further and it may be possible to compare the three types of mutations."
Generalisability	21	Discuss the generalisability (external validity) of the study results	10	Finally, although ADAD can serve as a model for sporadic AD, direct comparisons must explore potential differences.

Other information

Funding	22	Give the source of funding and the role of the funders for the present study and, if applicable, for the original study on which the present article is based	13	This research was funded by the National Institutes of Health (NIH) UFAG032438, UL1TR000448, P30NS098577, R01EB009352, the German Center for Neurodegenerative Diseases (DZNE), the National Institute for Health Research (NIHR) Queen Square Dementia Biomedical Research Centre, and the Medical Research Council Dementias Platform UK (MR/L023784/1 and MR/009076/1). DIAN ClinicalTrials.gov number, NCT00869817. We acknowledge the financial support of Fred Simmons and Olga Mohan, the

*Give information separately for cases and controls in case-control studies and, if applicable, for exposed and unexposed groups in cohort and cross-sectional studies.

Note: An Explanation and Elaboration article discusses each checklist item and gives methodological background and published examples of transparent reporting. The STROBE checklist is best used in conjunction with this article (freely available on the Web sites of PLoS Medicine at http://www.plosmedicine.org/, Annals of Internal Medicine at http://www.annals.org/, and Epidemiology at http://www.epidem.com/). Information on the STROBE Initiative is available at www.strobe-statement.org.